Gondwana Research 24 (2013) 1091–1107

Contents lists available at ScienceDirect

Gondwana Research

journal homepage: www.elsevier.com/locate/gr

Numerical modeling of eastern Tibetan-type margin: Influences of surface processes, lithospheric structure and crustal rheology

Lin Chen [a,b,*], Taras Gerya [b], Zhongjie Zhang [a], Guizhi Zhu [b], Thibault Duretz [b], Wolfgang R. Jacoby [c]

[a] State Key Laboratory of Lithospheric Evolution, Institute of Geology and Geophysics, Chinese Academy of Sciences, Beijing 100029, China
[b] Institute of Geophysics, Swiss Federal Institute of Technology (ETH Zurich), CH-8092 Zurich, Switzerland
[c] Institute fur Geowissenschafen, Johannes Gutenberg-Universität Mainz, D-59099 Mainz, Germany

ARTICLE INFO

Article history:
Received 16 August 2012
Received in revised form 26 December 2012
Accepted 8 January 2013
Available online 29 January 2013

Handling Editor: A.R.A. Aitken

Keywords:
Numerical modeling
Eastern Tibetan margin
Topography
Lithospheric structure
Partially molten crust

ABSTRACT

The eastern Tibetan margin is characterized by a steep topographic gradient and remarkably lateral variations in crustal/lithospheric structure and thermal state. GPS measurements show that the surface convergence rate in this area is strikingly low. How can such a mountain range grow without significant upper crustal shortening? In order to investigate the formation mechanism of the eastern Tibetan-type margins, we conducted 2D numerical simulations based on finite difference and marker-in-cell techniques. The numerical models were constrained with geological and geophysical observations in the eastern Tibetan margin. Several major parameters responsible for topography building, such as the convergence rate, the erosion/sediment rate, and the presence of partially molten crust, were systematically examined. The results indicate that the presence of partially molten material in the middle/lower crust can make a positive contribution to the formation of steep topography, but it is not a necessary factor. A steep topographic gradient may be a characteristic feature when a thin lithosphere with thick crust converges with a thick lithosphere with thin crust. In the context of a high erosion rate, the Longmen Shan range still gains and maintains its steep high topography to the present. This could be explained by exerting a large push force on Tibet side. Our numerical experiments suggest that topographic characteristic across the eastern Tibetan-type margins is mainly derived from isostatic equilibration forces and intensive convergence between two continental lithospheres with totally different rheological properties.

1. Introduction

It is widely believed that the Cenozoic collision between Eurasian and Indian plate has created the largest and highest plateau on Earth known as the Tibetan Plateau, although the starting time and process of the collision are still debated (Dewey et al., 1988; Molnar et al., 1993; Yin and Harrison, 2000; Johnson, 2002; Chung et al., 2005; Aitchison et al., 2007; Molnar & Stock, 2009; Aitchison et al., 2011; Searle et al., 2011; Xia et al., 2011; Dai et al., 2012; van Hinsbergen et al., 2012; Xu et al., 2012). The Tibetan Plateau is the largest region of high elevation (average 5023 m; Fielding et al., 1994) and extremely thick crust (60–70 km thick; Molnar, 1988; Zhang & Klemperer, 2010; Mechie et al., 2011; Zhang et al., 2010; Z. Zhang et al., 2011; Z.J. Zhang et al., 2011a, 2011b; Zhang et al., 2012) in the world. Despite its great elevation, the interior of the plateau is remarkably flat (Fielding et al., 1994).

In contrast to the flat hinterland, the eastern margin of the Tibetan Plateau, where the Longmen Shan (LMS) range marks the boundary between the Sichuan Basin and eastern Tibet, is characterized by a steep topographic transition separating the low-elevation Sichuan Basin and the high-elevation but low-relief plateau (Fig. 1). Although this margin is not the highest one among all margins surrounding the plateau, it exhibits the greatest topographic gradient among all the margins of the plateau, both at the moderate scale of individual mountain slopes and large scale of topography averaged over 10 km (Liu-Zeng et al., 2008). The elevation rises from ~500 m in the Sichuan Basin to over 4000 m in eastern Tibet, which occurs just over a distance less than 50 km across the LMS. In comparison with the Himalayas, the surface convergence rate across the LMS range revealed by GPS measurements is strikingly low (less than 3 mm/a) (Chen et al., 2000; Gan et al., 2007). If there is no significant young crustal shortening in the eastern Tibetan margin region, then how was the LMS built up? To date, several competing models have been proposed to understand its formation mechanism (Fielding and McKenzie, 2012). Tapponnier et al. (2001) presented crustal shortening model, which argues that thrust faulting and crustal shortening are the primary driver for the uplift of the LMS. Another popular proposal postulates that inflation of the ductile lower curst beneath the plateau edge by the lower crust channel flow

* Corresponding author at: State Key Laboratory of Lithospheric Evolution, Institute of Geology and Geophysics, Chinese Academy of Sciences, Beijing 100029, China. Tel.: +86 10 82998345; fax: +86 10 82998229.
E-mail address: chenlin@mail.iggcas.ac.cn (L. Chen).

1342-937X/$ – see front matter
http://dx.doi.org/10.1016/j.gr.2013.01.003

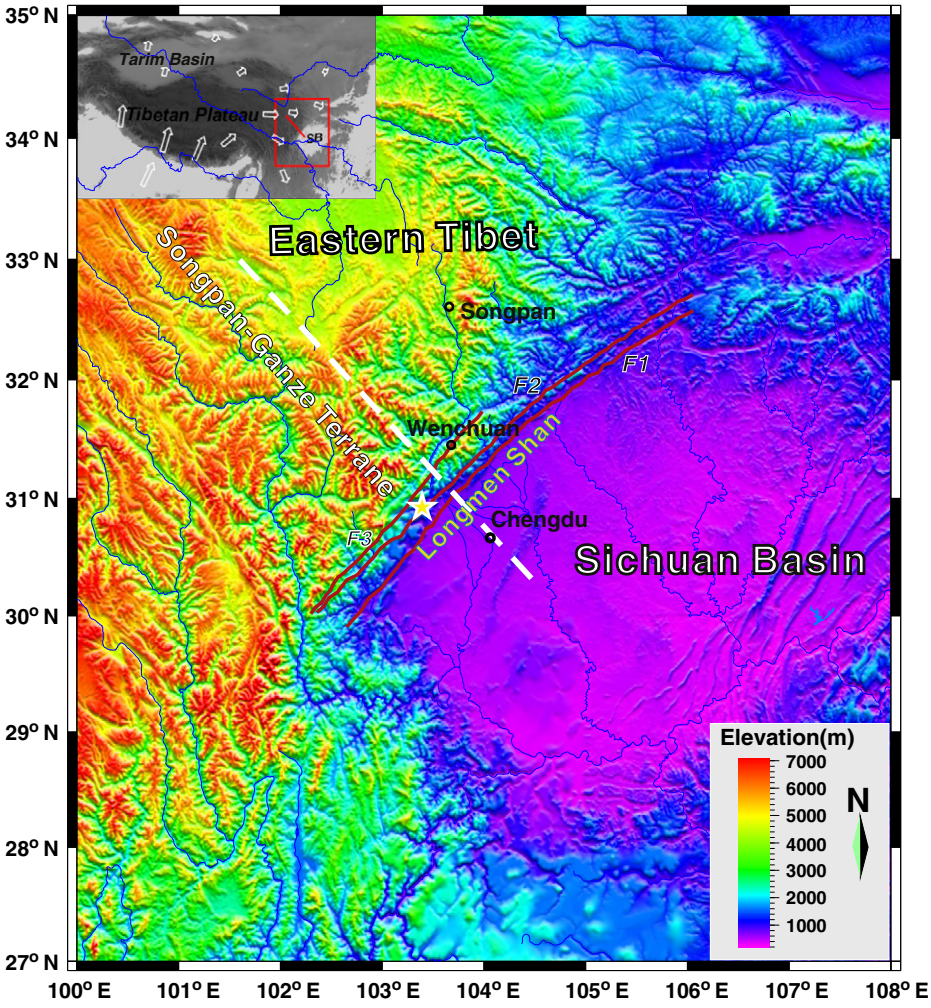

Fig. 1. Topographic map of the eastern margin of the Tibetan Plateau. The yellow star denotes the epicenter of the Wenchuan earthquake (Ms = 8.0). The red lines represent the main faults in this region. The dash white line indicates the location of an actual topography profile. The inset image in the top left corner is a map of the Tibetan Plateau and its surrounding area, in which arrows indicate GPS vectors (Gan et al., 2007).

evacuated from the central plateau leads to uplift of the LMS (Royden et al., 1997; Clark and Royden, 2000; Meng et al., 2006; Burchfiel et al., 2008). Although this model is compatible with a number of geophysical observations (Wang et al., 2007; Bai et al., 2010; Chen et al., 2012), it has been challenged by several recent studies. Hubbard and Shaw (2009) used balanced geologic cross sections to show that crustal shortening and topography are strongly correlated in the LMS front, which suggests that crustal shortening is a primary driver for the uplift of the LMS and lower crustal flow model is not required to produce this mountain range. A precise analysis of the Tibetan Plateau topography indicates that on the eastern margin some thrusts have localized the shortening and the topographic profile shows some steps corresponding to thrusts, not compatible with the prediction (smooth topography profile) of the lower crust flow model (Liu-Zeng et al., 2008).

Recent seismic studies reveal great variations in crustal and lithospheric structure exist between eastern Tibet and the Sichuan Basin (Wang et al. 2007; Robert et al. 2010; Zhang et al., 2009, 2010). The crustal thickness decreases from ~60 km beneath eastern Tibet to ~40 km beneath the Sichuan Basin with an abrupt Moho offset as large as 15–20 km beneath the LMS (Zhang et al. 2009; Robert et al. 2010). These observations suggest that there are significant crustal/lithospheric structural differences and likely rheological differences between the Sichuan Basin and eastern Tibet, and thus lead to an important question on the nature of mountain building processes: How can such a steep topography be attained and be maintained in the context of the collision of two plates with great differences in the crustal/lithospheric structure?

In order to address the above question, it is essential to explore how continental lithospheres with differing lithospheric architecture and rheological properties behave when subjected to convergence. Numerical modeling is the ideal approach to investigate this. Previously, numerous authors have explored the formation mechanism of the Tibetan Plateau with numerical modeling methods (England and McKenzie, 1982; England and Houseman, 1986; Houseman and England, 1993; Royden et al., 1997; Clark and Royden, 2000; Liu and Yang, 2003; Yang and Liu, 2009). However, such studies were generally based on a thin viscous sheet model or an assumption of a Newtonian fluid crust with different choices of rheology law and boundary conditions on stress and velocity. Although these models can explain some first-order observations, they cannot incorporate various well-constrained data into modeling and thus cannot account for more complex observations due to their oversimplification. In this study, we use a petrological–thermomechanical numerical code (i.e. I2VIS) developed by Gerya and Yuen (2003a), which can model complex realistic petrological and rheological behavior of the continental lithosphere, to investigate the formation mechanism of the eastern Tibetan-type margin. Unlike previous studies (Royden et al., 1997; Clark and Royden, 2000; Clark et al., 2005a), we constrain our

models with a variety of observations, including current crustal and lithospheric structure revealed by seismic methods, erosion and sediment rates derived from thermochronological studies, and rheological parameters extrapolated from laboratory studies. The modeling results are assessed by comparing model-predicted topographies to an observed topography profile across the LMS (see Fig. 1).

2. Numerical model

2.1. Geological and geophysical basis for the model setup

2.1.1. Hot eastern Tibet and cold Sichuan Basin

P-wave tomography reveals a seismically fast structure beneath the Sichuan Basin extending to ~250 km depth (Li et al., 2006, 2008), which indicates that the basin is underlain by a deeply rooted, probably cold, craton-like lithosphere. In contrast, above ~250 km depth, the eastern Tibet region is seismically slow, probably reflecting lower mechanical strength and elevated temperatures in the lithosphere (Li et al., 2006, 2008, 2012a). Alkali-rich magmatic rocks that were erupted in this region from early Cenozoic to Pliocene time have melt temperatures in excess of ~1300 °C at depths of 80–100 km, indicating anomalously high temperatures at the base of, and probably throughout, the crust of the eastern Tibetan Plateau (Holbig & Grove, 2008). Therefore, the lithosphere beneath eastern Tibet has probably been quite thin throughout the Cenozoic. Recent heat flow measurements in the region show that the heat flow in eastern Tibet can reach 95 mW/m^2, while the heat flow in the Sichuan Basin only ranges from 35.4 to 68.8 95 mW/m^2 with an average of 53.2 mW/m^2 (Yuan et al., 2006; Xu et al., 2011). In addition, 2-D flexural modeling shows the effective elastic thickness of the lithosphere beneath eastern Tibet is much lower than that beneath the Sichuan Basin (Braitenberg et al., 2003; Jiang and Jin, 2005; Fielding and McKenzie, 2012). These observations together with the fact that the Sichuan Basin was mostly not affected by the Mesozoic and Cenozoic deformations that affected the surrounding zones (Burchfiel et al., 1995) suggest that the lithosphere beneath the Sichuan Basin is cold and mechanically strong compared to eastern Tibet. According to these observations, we designed the model setup to ensure that the geothermal gradient (cf. distribution of isotherms in Fig. 2) for the left side representing eastern Tibet (Songpan-Ganze terrane) is hotter than the one for right side representing the Sichuan basin.

2.1.2. Crustal and lithospheric structure

Recent seismic studies carried out in eastern Tibetan margin provide detailed information on crustal and lithospheric velocity and structure (Wang et al., 2007; Zhang et al., 2009; Zhang et al., 2010; Robert et al., 2010). A low seismic velocity zone is commonly found in the crust beneath the eastern Tibet, while this low velocity zone does not appear in the crust of the adjacent Sichuan Basin (Wang et al., 2007; Lei and Zhao, 2009). This is considered as an important evidence for the existence of a lower crustal channel beneath the eastern Tibet. The crustal thickness decreases from ~60 km beneath eastern Tibet to ~40 km beneath the Sichuan Basin. There is an abrupt 15–20 km Moho offset directly below the LMS (Zhang et al., 2009; Robert et al. 2010), which marks the boundary between the eastern Tibet and the Sichuan Basin. A recent seismic receiver function study shows that the lithospheric thickness beneath the eastern Tibet is about 30 km thinner than beneath the Sichuan Basin (Zhang et al. 2010). Zhang et al. (2010) suggested that the eastern Tibetan mantle lithosphere might have been partially removed by convective flow of the underlying asthenosphere. This convective-removal model may provide a heating mechanism for the presence of a weak middle/lower crust beneath eastern Tibet assumed in our model (cf. lithological structure of the model in Fig. 2) and perhaps also cause some surface uplift due to the isostatic rebound. The observations of the crustal/lithospheric structure in the LMS region provide solid constraints on our model setup.

It should be pointed out that the initial configuration of our model is established on the basis of the present-day rather than past crustal/lithospheric structure in the eastern Tibetan margin region. In the absence of firm constraints on the past lithospheric structure beneath eastern Tibet, its current structure has been used as a guide to the past. Although we cannot be certain of past lithospheric structures, the following arguments support the validity of our model:

1) The Sichuan Basin is the western part of the Yangtze craton, and geological observations demonstrate that the Sichuan Basin was mostly not affected by the Mesozoic and Cenozoic orogeny that affected the surrounding regions (Burchfiel et al., 1995). Therefore, we have good reason to justify that the crustal architecture of the Sichuan Basin before the uplift of the Longmen Shan was basically similar to its present-day structure.
2) The focus of our study is to investigate the formation mechanism of the eastern Tibetan margin topography with numerical modeling method, thus the models are supposed to evolve from the beginning of the uplift of the LMS. According to a series of low-temperature thermochrological studies carried out in the Longmen Shan and adjacent regions, the present high topography of the Longmen Shan and the eastern Tibetan Plateau was not developed until the Late Cenozoic (Arne et al., 1997; Kirby et al., 2002; Clark et al., 2005b; Burchfiel et al., 2008; Godard et al., 2009a, 2009b; Li et al., 2012b; Wang et al., 2012). Furthermore, Wallis et al. (2003) demonstrated the existence of a previously unknown region of ca. 65 Ma Barrovian-type metamorphism in central Longmen Shan, suggesting that the crust beneath the Longmen Shan was already thick at the time of the India–Asia collision and only minor post-collisional deformation is needed to account for the present thickness, which indicates that the crust

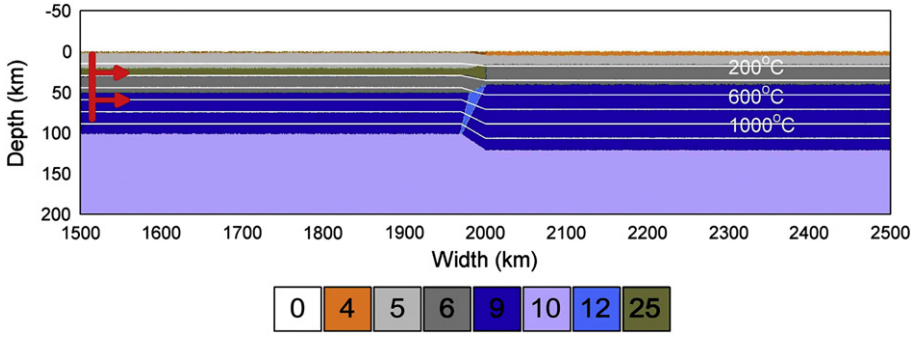

Fig. 2. Reference model. The color code represents the different rock types, with: 0-sticky air; 4-sediment; 5-upper continental crust; 6-lower continental crust; 9-lithospheric mantle; 10-asthenosphere; 12-weak zone mantle; 25-partially molten continental crust. The red arrow denotes the direction of convergence force. White lines are isotherms measured in Celsius.

beneath eastern Tibet has probably been thickened before the uplift of the LMS. Although it is still controversial that high-grade metamorphism indicates crustal thickening (Maidment et al., 2013), we follow their interpretation as a guide to the past crustal structure beneath eastern Tibet.

2.1.3. Properties of weak lower crust

The steep topography of the eastern plateau margin was previously supposed to be the direct result of crustal thickening by weak, lower crustal material evacuated from beneath the central plateau (Royden et al. 1997; Clark & Royden, 2000). Gradients in crustal thickness varying from ~70 km thick beneath the central plateau to the ~35 km thick beneath the Sichuan basin are considered to be the driving force for lower crust flow (Clark et al., 2005a).

According to recent seismic (Wang et al., 2007, 2010; Bai et al., 2011) and magnetotelluric studies (Bai et al., 2010) in this region, there are low seismic velocity and high electrical conductivity zones at middle/lower crustal level in eastern Tibet. These observations are considered as strong evidences for the capability of the lower crust flowing beneath eastern Tibet. It was inferred that the low velocity and high conductivity zones found in the middle/lower crust are composed of partially molten material with low viscosity (Royden et al., 1997; Burchfiel et al., 2008). Thus, its mechanical strength is supposed to be weak. Despite some authors had estimated the viscosity of the lower crust beneath the eastern Tibet, which varied from 10^{18} to 10^{21} (Clark and Royden, 2000; Clark et al., 2005a; Copley and McKenzie, 2007), many other properties of this weak layer are not yet well understood. Its origin, if it really exists, is unclear as well. Thus, in this study, we explore two end members, one containing a partially molten felsic layer within the middle/lower crust (cf. greeny brown-colored crustal region in Fig. 2), the other without such a layer, to investigate its effect on the topography building. In our model, a partially molten felsic crust spontaneously has a low viscosity and weak mechanical strength due to its realistic rheological properties (see Table 3).

2.2. Numerical method

The numerical investigations were conducted in two dimensions using the petrological–thermomechanical code I2VIS (Gerya and Yuen, 2003a, 2007). This code solves the momentum and heat equation based on staggered grid conservative finite differences and a non-diffusive marker-in-cell technique taking into account realistic visco-plastic rheologies (Gerya and Stockhert, 2006). This methodology has been widely applied to the numerical modeling of a variety of geodynamic problems (Gerya et al., 2004a, 2004b; Gerya & Stockhert, 2006; Gerya et al., 2008; Duretz et al., in press). A thermodynamic database is implemented in the code and accounts for phase transformations and partial melting for different lithologies. A detailed description of the equations and numerical techniques employed in our study is given in Appendix A.

The experiments were performed in a 4000∗1500 km domain. The non-uniform 1361∗351 rectangular grid is designed with a resolution varying from 1∗1 km in the zone of interest (i.e. the interacting zone between the two lithospheric domains in Fig. 2) to 10∗10 km in the zones beside it. The velocity boundary conditions are free slip at all the boundaries, except at the lower boundary, which is treated as a permeable boundary satisfying an external (i.e. remote) free slip boundary condition (Burg and Gerya, 2005). The upper thermal boundary is set to a constant temperature and the lower thermal boundary is set to an external constant temperature condition that simulates an additional mantle volume present below the bottom of the model. Both lateral thermal conditions are insulating.

The top surface of the crust is calculated dynamically as an internal quasi free surface by employing a sticky air layer of low viscosity (10^{19} Pa s) and low density (1 kg/m^3). The validity of this weak layer approach for approximating the free surface has recently been tested and confirmed (Schmeling et al., 2008). The interface between this weak layer and the top of crust deforms spontaneously and is treated as an internal erosion-sediment surface that evolves according to the transport equation solved (gross-scale erosion-sediment law) at each time step (Gerya and Yuen, 2003b, also see Appendix A). In this manner, topography can spontaneously grow and evolve with time.

3. Results

Eleven numerical experiments were performed to investigate the influence of: (1) the convergence rate; (2) the erosion/sediment rates and (3) the existence of partially molten middle/lower crust on mountain building. The configurations and parameters are shown in Tables 1 and 2.

3.1. Reference model

The lithology structure of the reference model (see Fig. 2) was designed mainly based on results derived from the seismic studies performed in eastern Tibet region. A number of evidences indicate that the eastern Tibet block (Songpan-Garze terrane) is significantly different from the Sichuan Basin both in structure and composition and such differences might have existed throughout the Cenozoic (Yin, 2010). The crustal thickness and thermal state in eastern Tibet were inherited from the Tibetan Plateau, while the Sichuan Basin is a stable stiff block and didn't deform much during Cenozoic (Burchfiel et al., 1995). Therefore, the differences between these two blocks have existed for a long time. Geological observations demonstrate that there are four sub-parallel NE-SW trending thrust faults separating eastern Tibet from the Sichuan basin in front of the Longmen Shan (Burchfiel et al., 1995; see Fig. 1). In order to keep consistent with geological observations and distinguish these two different lithospheres at depth, we impose a weak zone in the mantle between the two plates (Fig. 2). The dip angle of the weak zone is grossly consistent with the observed thrust fault (Burchfiel et al., 2008). We also tested a model without such a weak zone. It was observed that the weak zone just slightly affects the initial temperature field, but it has no significant influence on the build-up of the topography. For geological consistency, we keep such a weak zone in our models.

The thickness of the sticky air used in the model is 50 km, which is chosen to avoid the potential traction effect of the sticky air (Schmeling et al., 2008). The left part of the reference model, representing the eastern Tibet, is composed of a 1 km-thick sediment layer, a 19 km-thick quartzite upper crust, a 10 km-thick partially molten middle crust (wet quartzite, see Table 3), a 20 km-thick lower crust and 50 km-thick lithospheric mantle, while the right part of the reference model, representing the Sichuan Basin, is composed of a 4 km-thick sediment layer, 11 km-thick upper crust, a 25 km-thick lower crust, and a 80 km-thick lithospheric mantle (Fig. 2). The rheological parameters of each layer are shown in Table 3. A fixed convergence rate (2.5 cm/a), which was varied in

Table 1
Description of numerical experiments.

Model name	Weak zone	Convergence rate (cm/a)	Erosion rate (mm/a)	Sediment rate (mm/a)	Partially molten crust
chan01	Yes	2.5	0.5	0.3	Middle crust
chan02a	Yes	2.0	0.5	0.3	Middle crust
chan02b	Yes	1.5	0.5	0.3	Middle crust
chan02c	Yes	1.0	0.5	0.3	Middle crust
chan02d	Yes	0.5	0.5	0.3	Middle crust
chan03a	Yes	2.0	0.0	0.0	Middle crust
chan03b	Yes	2.0	1.0	0.6	Middle crust
chan03c	Yes	2.0	0.8	0.6	Middle crust
chan03d	Yes	2.0	0.6	0.6	Middle crust
chan04	Yes	2.5	0.5	0.3	No
chan05	Yes	0.0	0.0	0.0	Middle crust

Table 2
Material properties used in the numerical experiments (Gerya, 2010). Other properties (for all rock types): $C_p = 1000$ J kg^{-1} K^{-1}, $\rho = \rho_0[1-\alpha(T-T_0)]\times[1+\beta(P-P_0)]$, where $\alpha = 3\times10^{-5}$ K^{-1} is thermal expansion, $\beta = 1\times10^{-5}$ MPa^{-1} is compressibility, ρ_0 is standard density at $T_0 = 298$ K and $P_0 = 0.1$ MPa. All the local rock properties (density, heat capacity and thermal expansion) are updated at each timestep according to Gibbs energy minimization (Gerya et al., 2004b).

Material	ρ_0, kg/m3	Thermal conductivity k, W/(m K)	$T_{solidus}$, K	$T_{liquidus}$, K	Q_L, kJ/kg	H_r, μWm3
Sediment	2600	[0.64 + 807/(T + 77)]	889 + 17900/(P + 54) + 20200/(P + 54)^2 at P<1200 MPa, 831 + 0.06P at P>1200 MPa	1262 + 0.09P	300	1.5
Upper continental crust	2700 (solid) 2400 (molten)	[0.64 + 807/(T + 77)]	889 + 17900/(P + 54) + 20200/(P + 54)^2 at P<1200 MPa, 831 + 0.06P at P>1200 MPa	1262 + 0.09P	300	1.0
Lower continental crust	2800 (solid) 2500 (molten)	[1.18 + 474/(T + 77]	973–70400/(P + 354) + 77800000/(P + 354)^2 at P<1600 MPa, 935 + 0.0035P + 0.0000062P^2 at P>1600 MPa	1423 + 0.105P	380	0.25
Lithosphere–asthenosphere dry mantle	3300 (solid) 2700 (molten)	[0.73 + 1293/(T + 77]×(1 + 0.00004P)	1394 + 0.132899P-0.000005104P^2 at P <10000 MPa 2212 + 0.030819(P-10000) at P>10000 MPa	2073 + 0.114P	400	0.022
Lithosphere–asthenosphere hydrated mantle	3200 (solid) 2700 (molten)	[0.73 + 1293/(T + 77]×(1 + 0.00004P)	1240 + 49800/(P + 323) at P<2400 MPa, 1266–0.0118P + 0.0000035P^2 at P>2400 MPa	2073 + 0.114P	400	0.022

different numerical experiments (see Section 3.2), is imposed only at the left margin of the Tibet plate, while the right plate is immobile at the beginning.

Fig. 3 shows the evolution of the reference model (i.e., chan01 in Table 1). The crust and lithosphere on the left side are visibly thickened and buckled due to the obstruction of the rigid Sichuan plate on the right side (see Fig. 3a′–c′). A fold-and-thrust structure is formed within the upper crust at the conjunction zone between the two plates (Fig. 3), which is consistent with the interpretations of the seismic reflection profiles across the LMS (Li et al., 2010). The partially molten middle crust is accumulated at the interface of the two parts and moves upward (see Fig. 3b′–c′) at the later stages.

Because the left side is initially set to be hotter than the right side, the viscosity on the left side is lower than that at a similar depth on the right side, especially at the level of the middle crust in the left part where the material is partially molten due to the hotter geothermal gradient (see Fig. 3a). Cook and Royden (2008) mentioned that an important consequence of the existence of a weak lower crust is the potential decoupling between the mantle and the upper crust. However, our modeling demonstrates that the presence of a partially molten middle crust, which has a low viscosity relative to the surrounding material, does not unambiguously cause the decoupling of the upper crust from the lower crust (see velocity vectors shown in Fig. 3b–c). This is consistent with the result revealed by seismic anisotropy studies, showing the deformations of the crust and lithospheric mantle are coupled in the eastern Tibet region (Lev et al., 2006; Wang et al., 2008; Chen et al., 2012). Several authors have estimated viscosity of crust channel flow quantitatively (Clark and Royden, 2000; Clark et al., 2005a; Copley and McKenzie, 2007). Clark et al. (2005a) obtained the value of 10^{21} Pa.s for the eastern Tibet margin. The viscosity values at mid crustal level on the left side, shown in Fig. 3a–c, are consistent with this estimation. Furthermore the viscosity in the middle crust here evolves with time and is pressure- (i.e. depth-) and temperature-dependent rather than having a constant value for the whole crust channel (Clark and Royden, 2000).

The continuous convergence, where the convergence rate is 2.5 cm/a, between these two blocks produces contrasting topographies, as shown in Fig. 4a. The topography builds up rapidly at the beginning, which reaches ~2.0 km in less than 1 Myr (see Fig. 4a). We also compare predicted topographies at different times with an actual topographic profile across the eastern Tibetan margin (see Fig. 4b), whose location is shown in Fig. 1. As the push exerted on the left side moves forward, the topography grows continuously and propagates to the right (see Fig. 4c). We also observe shape similarities between the observed and modeled topographies (see Fig. 4b). Specifically, they both have a steep topographic gradient at the interface between the two blocks on the same horizontal distance scale, although the magnitude doesn't match quite well. For further comparison, we calculate the topographic slope of the observed topography and modeling topographies (see Fig. 5). The slopes of the reference model at different times all have two peaks (see Fig. 5b). It could grow up to 15.2° just in 4.448 Myr (starting from the model run, the same below; see the red solid line in Fig. 5b). The maximum value of slopes constantly increases before ~20.448 Myr (see Fig. 5b). After that, the slope starts to decay due to the long time accumulation of sedimentation (see Figs. 4c and 5b). Because of the intensive fluctuation of the actual topography profile, there are many peaks on the slope of the actual topography (see Fig. 5a). But the modeling results are comparable to the slope magnitude at the mountain front.

3.2. The effect of the convergence rate

This type of model differs from reference model by having a higher/lower convergence rate. The other parameters are the same as the reference model (see Table 1). Because the evolution of the composition and viscosity fields are similar to those in the reference model, we just show the topographies here. The convergence rates are reduced from 2.5 cm/a to 0.5 cm/a with a step of 0.5 cm/a. The topographies throughout the simulations with different convergence rates are shown in Fig. 6. We observe that the maximum height of the topography is reached on the left side and decreases with decreasing convergence rate (see Fig. 6b–f). If the convergence rate is high (2.5 cm/a), the topographic peak is achieved at a later stage (see Fig. 6b). When the convergence rate is less than 2.0 cm/a, the

Table 3
Rheological parameters of material used in this study. η is the reference viscosity; n is the stress exponent; E_a is the activation energy; V_a is the activation volume; ϕ is the friction angle; C is the cohesion.

Material	Flow law	η(MPa^n S)	n	E_a(J)	V_a(J/bar)	sin(ϕ)	C (MPa)
Sediment	Wet quartzite	1.97×10^{17}	2.3	1.54×10^5	0.8	0.15	1
Upper continental crust	Wet quartzite	1.97×10^{17}	2.3	1.54×10^5	0.8	0.15	1
Lower continental crust	Plagioclase (An75)	4.80×10^{22}	3.2	2.38×10^5	1.2	0.15	1
Partially molten crust	Wet quartzite	5.00×10^{14}	1.0	0.00	0.0	0.00	1
Mantle	Dry olivine	3.98×10^{16}	3.5	5.32×10^5	0.8	0.60	1
Weak zone	Wet olivine	5.01×10^{20}	4.0	4.70×10^5	0.8	0.00	1

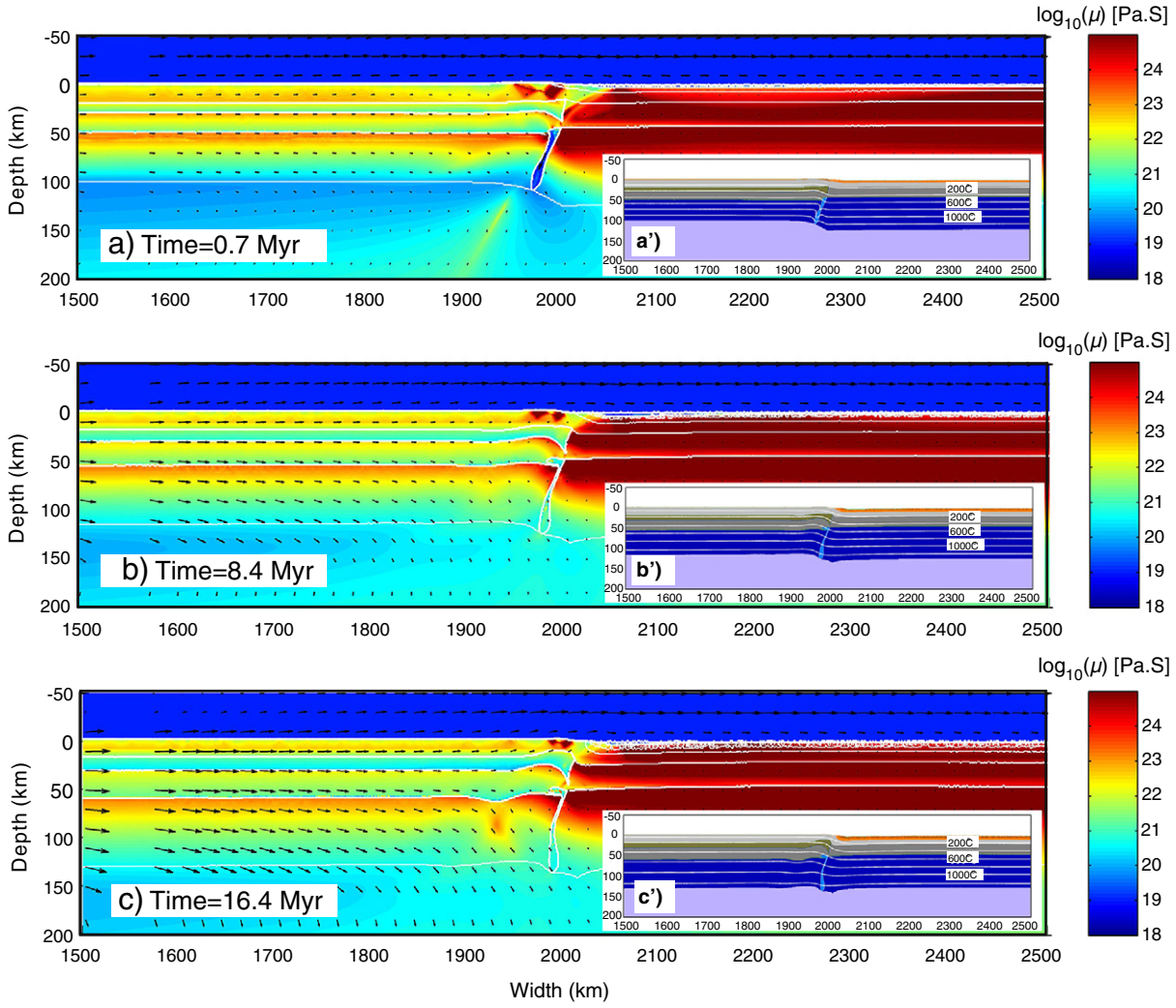

Fig. 3. The composition and viscosity evolution of the reference model. Color bars to the right side indicate the magnitude of the viscosity in logarithm. Black arrow indicates the velocity vector and the white lines denote composition contour. The inset images show the composition fields for the same domain with white numbered isothermal lines in °C. The color code of the composition field is the same as in Fig. 2.

topographic peak appears at a very early stage (less than 1 Myr) (see Fig. 6c–f). When the convergence rate is less than 1.0 cm/a, the altitude reaches its maximum in ~1 Ma. After this period, the erosion starts to play a dominant role and the topography starts to decay with time (see Fig. 6e–f). Therefore, the convergence rate is a very important factor for the build-up of topography. If the convergence rate is greater than 2.5 cm/a, the topography can keep growing. When the convergence rate is less than 1.0 cm/a, its positive effect on mountain building may be replaced by erosion. During the topography building process, the constructive effect of convergence competes with the destructive effect of erosion. In the following section, we will further discuss the effect of erosion and sedimentation. Although the GPS measurement shows that present surface convergence rate in the LMS area is less than 3 mm/a, recent convergence rates in the upper crust are not necessarily indicative of the long-term, large-scale lithospheric convergence rate (Chen et al., 2012). Thus, the surface convergence rates do probably not represent the actual gross-scale convergence rates (lithospheric shortening rates) in the eastern Tibet region. From the above numerical simulations, we would expect it to be at least one order of magnitude greater than the actual surface convergence rate. In particular, Fig. 4 indicates that the rate of topography displacement to the right is one order of magnitude lower (about 2 mm/a) compared to the imposed convergence rate (2.5 cm/a). This can be explained by the rigidity of the right plate that remains basically undeformed while the convergence is mainly accommodated by thickening and buckling of the rheologically weak left plate (see Fig. 3).

3.3. The effect of erosion/sediment rate

Erosion and sedimentation processes play an important role in the evolution of a continental collision zone (Avouac and Burov, 1996; Willett, 1999; Pysklywec, 2006; Godard et al., 2009a). As pointed out by Pysklywec (2006) and Gerya et al. (2008) in the case of subduction and collision, variations in erosion/sediment rates may significantly affect the crustal mass flux and consequently alter the behavior of the crust-mantle interface. In this series of models, we vary erosion/sediment rate systematically to check their effect on the topography. Apart from the erosion/sediment rates, the other parameters (see Tables 1 and 2) are kept the same as in the reference model. It is noteworthy that the erosion/sediment rates used here are consistent with the estimations reported by Kirby et al. (2002), Lai et al. (2007), and Godard et al. (2009b).

First, we investigate the topographic development in the absence of erosion/sediment, as shown in Fig. 7, in which the erosion and sediment rates are both set to be zero. The convergence rate is 2.0 cm/a. It is found that although the topography on the right side constantly increases with time, its uplift rate gradually decreases after a period of ~17.9 Myr (see Fig. 7c). The shape of the topography resembles that of the observed

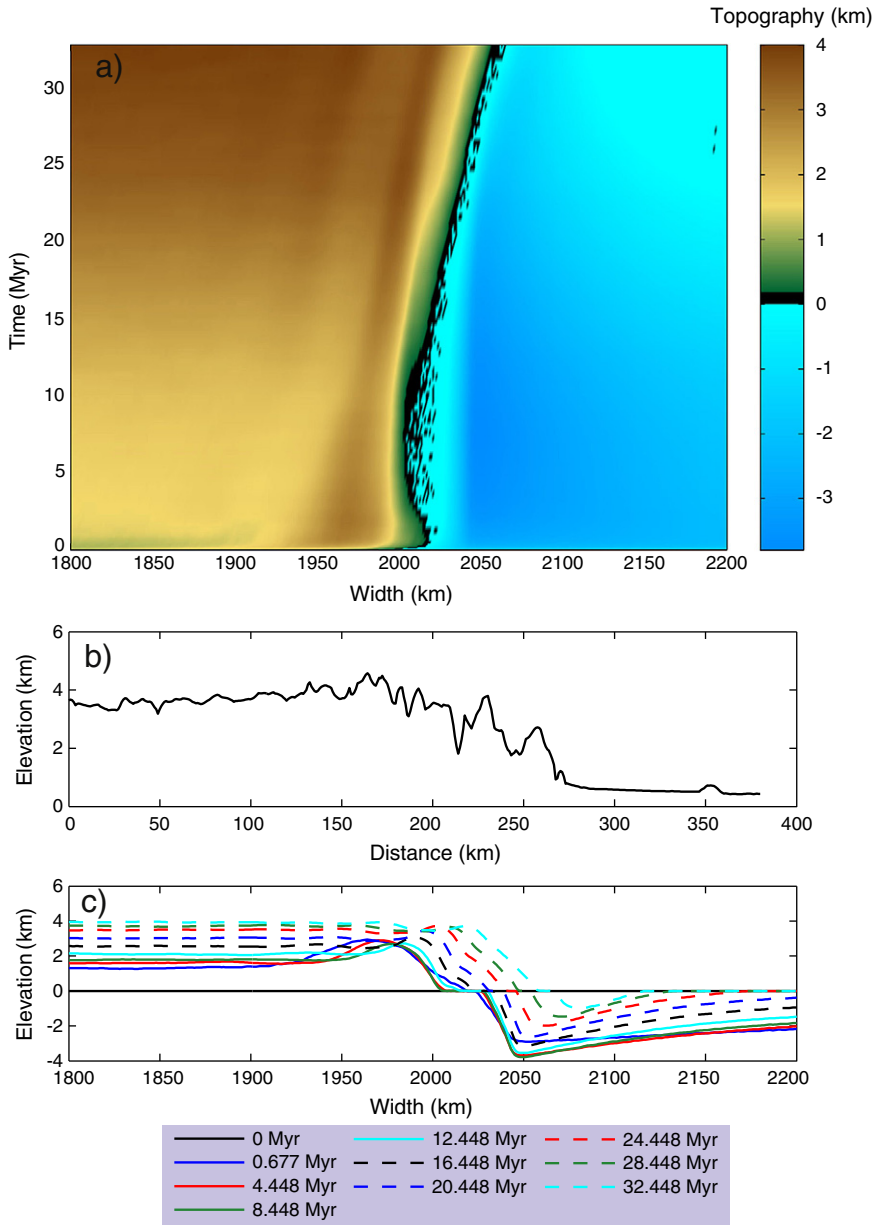

Fig. 4. The topography development of the reference model. (a) The topography evolution with time (counting from the start of modeling, the same below). Colors indicate the magnitude of topography in km. (b) An actual topography profile across the eastern Tibetan margin. The location of the profile is shown in Fig. 1. (c) The topography profiles of the reference model at different times.

one (see Fig. 7a–b). The slope keeps on moving to the right with the velocity of around 2 mm/a due to the push exerted on the left side (see Fig. 7b). The model-predicted uplift rates, which basically decrease with modeling time, range from 0 to ~170 m/Myr (e.g. Fig. 7c). Burchfiel et al. (2008) estimated that the long-term gross uplift rates are ~0.3-0.8 mm/yr by dividing the topographic relief across the LMS (~4 km) by the estimated initiation age for surface uplift (ca. 5–12 Ma). According to a more recent thermochronological study conducted by Wang et al. (2012) in the eastern Tibetan margin, the surface uplift of the LMS initiated from 30 to 25 Ma ago. If the 4 km high topography is divided by 30 Ma, we can obtain a gross uplift rate of ~130 m/Ma, which is consistent with the prediction of our model.

In the next three models, the sediment rate is fixed to 0.6 mm/a, and the erosion rate is reduced from 1.0 mm/a to 0.6 mm/a with a step of 0.2 mm/a. The convergence rate is the same as in the previous model (2.0 cm/a). The evolution of the topography is shown in Fig. 8. We observe that when the erosion rate is large, the topography achieves its maximum at the very beginning of the experiment; after that, the topography keeps decreasing and approaching the sea level (see Fig. 8b). This can be explained by considering the competition existing between the tectonic contribution and the erosion in the development of topography. When the erosion rate is decreased to 0.8 mm/a, these two forces are almost in balance, and the topography is almost constant with time (see Fig. 8c). As the erosion rate drops to 0.6 mm/a, the tectonic forcing plays a predominant role. The topography keeps uplifting but the uplift rate slows down, approaching zero, throughout the simulation time (see Fig. 8d). In the above three cases, the depressions formed at the edge of the right side all are filled up and almost reach the sea level at a later stage. Erosion provides material for sedimentation. Therefore, these two processes are closely linked.

The LMS range is located in the Southeast Asian and South Asian monsoon zones. The precipitation is ample in this region (Wang and Meng, 2009). There are many rivers crossing this region, such as Jinsha River, Dadu River, Mingjiang River and so on. Kirby et al. (2002)

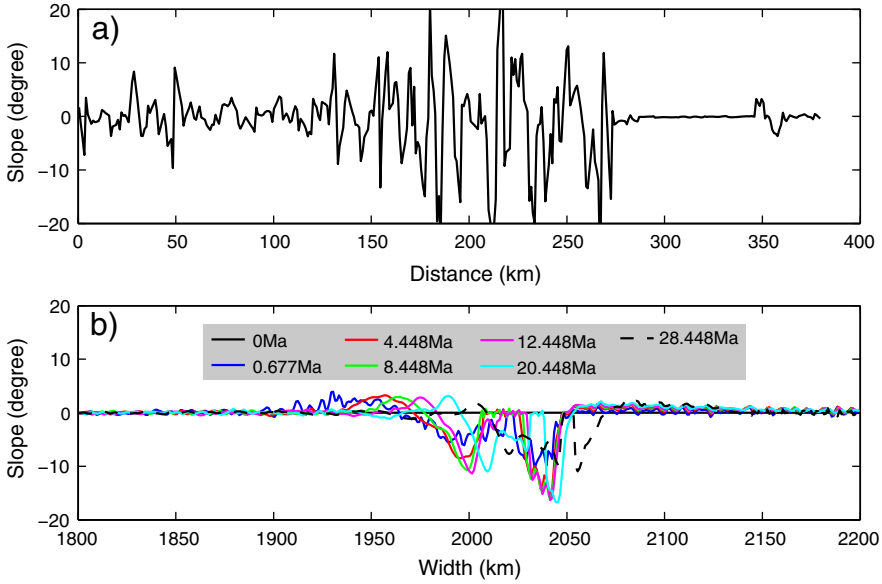

Fig. 5. A comparison of topographic slope between an actual topography profile and modeled topographies. (a) The slope of an actual topography profile across the eastern Tibetan margin, whose location is shown in Fig. 1. (b) The slopes of modeling topographies at different times.

estimated the erosion rate at the topographic front of the LMS up to 1–2 mm/a during 12 to 5 Ma based on an integrated $^{40}Ar/^{39}Ar$ and (U–Th)/He dating of samples along the eastern margin of the Tibet Plateau. Clark et al. (2005b) determined the erosion rates (0.25–0.5 mm/a) and initiation age of rapid erosion (9–13 Ma) based on thermochronological studies in southeast Tibet region, which is consistent with their previous results (Kirby et al., 2002) obtained in the northwest of the study area. Lai et al. (2007) suggested that the eastern Tibetan Plateau has experienced two-step rapid cooling respectively corresponding to ~20–16 Ma and ~5 Ma since Cenozoic based on the apatite fission track thermochronologcial study in this region. They estimated an average erosion rate of ~0.4 mm/a. Godard et al. (2009b) showed that a major phase of exhumation started at 8–11 Ma with an average rate of ~0.65 mm/a according to (U–Th)/He thermochronological dating derived from central Longmen Shan, eastern Tibet. More recently, Liu-Zeng et al. (2011) used sediment load data from hydrographic stations on rivers across the LMS

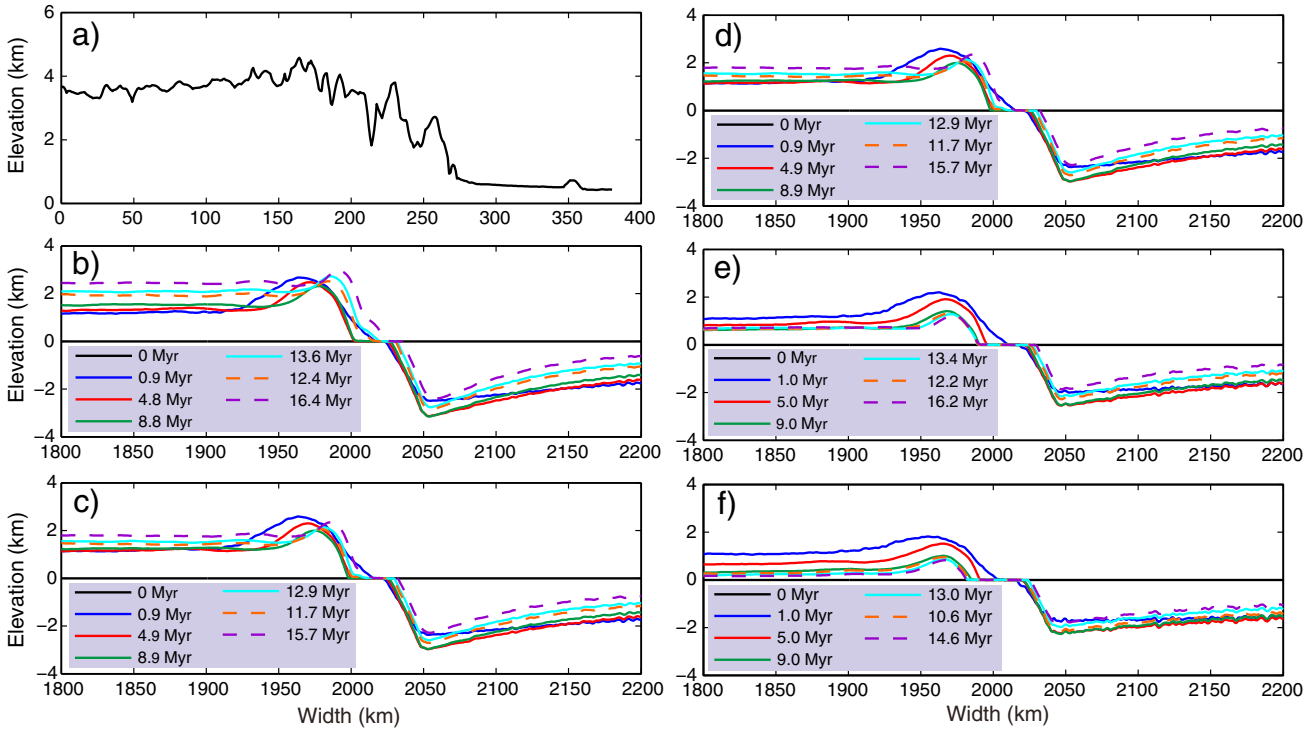

Fig. 6. The comparison between an actual topography and modeled topographies. (a) An actual topography profile across the eastern Tibetan margin. The location of the profile is shown in Fig. 1. The topography profiles at different times with a convergence rate of (b) 2.5 cm/a; (c) 2.0 cm/a; (d) 1.5 cm/a; (e) 1.0 cm/a and (f) 0.5 cm/a.

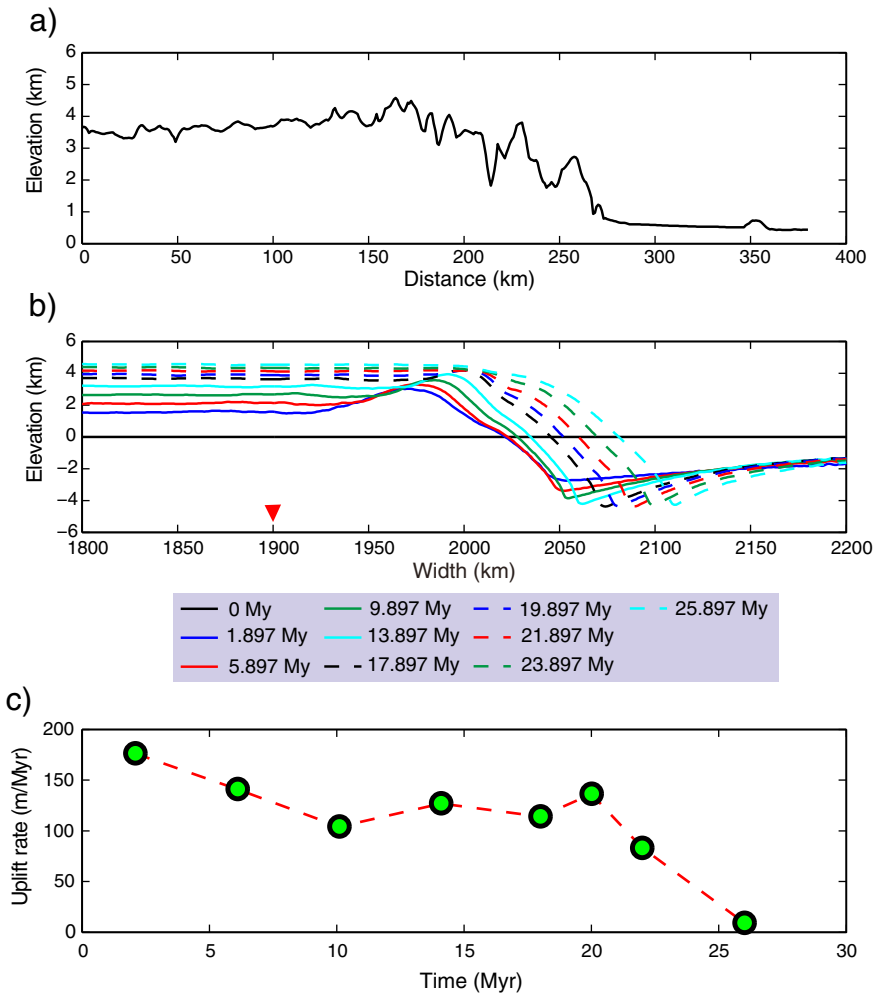

Fig. 7. The comparison between an actual topography and modeled topographies. (a) An actual topography profile across the eastern Tibetan margin. The location of the profile is shown in Fig. 1. (b) The topography profiles at different times (with zero erosion and sediment rate). The inverse red triangle indicates the location of the evolution of uplift rate in Fig. 8c. (c) The evolution of uplift rate at 1900 km.

to evaluate the pattern of denudation rate in the region, and delineated a zone of relatively high erosion rate (~0.5 mm/a) adjacent to the margin bounding active reverse faults, and a decrease with increasing distance plateauward, to 0.05 mm/a at 200 km distance. Although the results reported by different authors are different, the overall erosion rate in eastern Tibet region is relatively high. From the above numerical experiments, it is found that when erosion rate is greater than 1.0 mm/a, the topography built-up by tectonic forces at the beginning keeps going down and breaks down at a later stage. In this case, the topography cannot be maintained. A simple dimensional analysis (Gratton, 1989) and numerical simulations (Bird, 1991) of lateral extrusion of lower crust resulted from an effective lateral pressure gradient of topography load show that the topography as high as 3500 m with a range of 300–400 km wide should be collapsed by half in a few million years or at most tens of millions of years, depending on the assumed rheology of the lower crust. The LMS range is right situated in the context of high erosion rate, but its steep topography is preserved to the present. This demonstrates that the tectonic force (expressed by convergence rate in our models) must be great enough to counteract the destructive effects of the high erosion rate and lateral flow of crust root. If the average erosion rate in this region is no less than 0.8 mm/a, the actual gross-scale lithospheric convergence rate (lithospheric shortening rate) should be greater than 2.0 cm/a in order to build up and maintain the steep topography.

3.4. The effect of the partially molten crust

In this model, we investigate the influence of the presence of partially molten crust on topographic build up. In contrast to the reference model, the partially molten middle crust is replaced by plagioclase lower crust in this model. The related parameters used in this model can be found in Tables 1 and 2. Fig. 9 shows the evolution of the composition and viscosity field with time. The lower crust is thickened and buckled due to indenting effect of the mechanically strong Sichuan Basin (see Fig. 9a′–c′). Again, a fold-and-thrust structure within the upper crust is formed at the conjunction zone to the eastern Tibet side (Fig. 9b′–c′). Even if the left part of the model is now composed of felsic plagioclase material, the viscosity of lower crust on the left side is still relatively low due to its high geothermal gradient (see Fig. 9a–c). Despite the absence of partially molten crust, the compression still leads to a steep topographic gradient (see Fig. 10), which is also comparable to that of the observed topography. A distinct difference is that the topography on the left side is now characterized by two big bulges (see Fig. 10b), which are caused by buckling of the crust.

To further investigate what causes the topography, a new model is specially designed to check the effect of partially molten crust separately, in which the convergence rate, the erosion rate and the sediment rate are all set to zero and only keep the partially molten crust. The

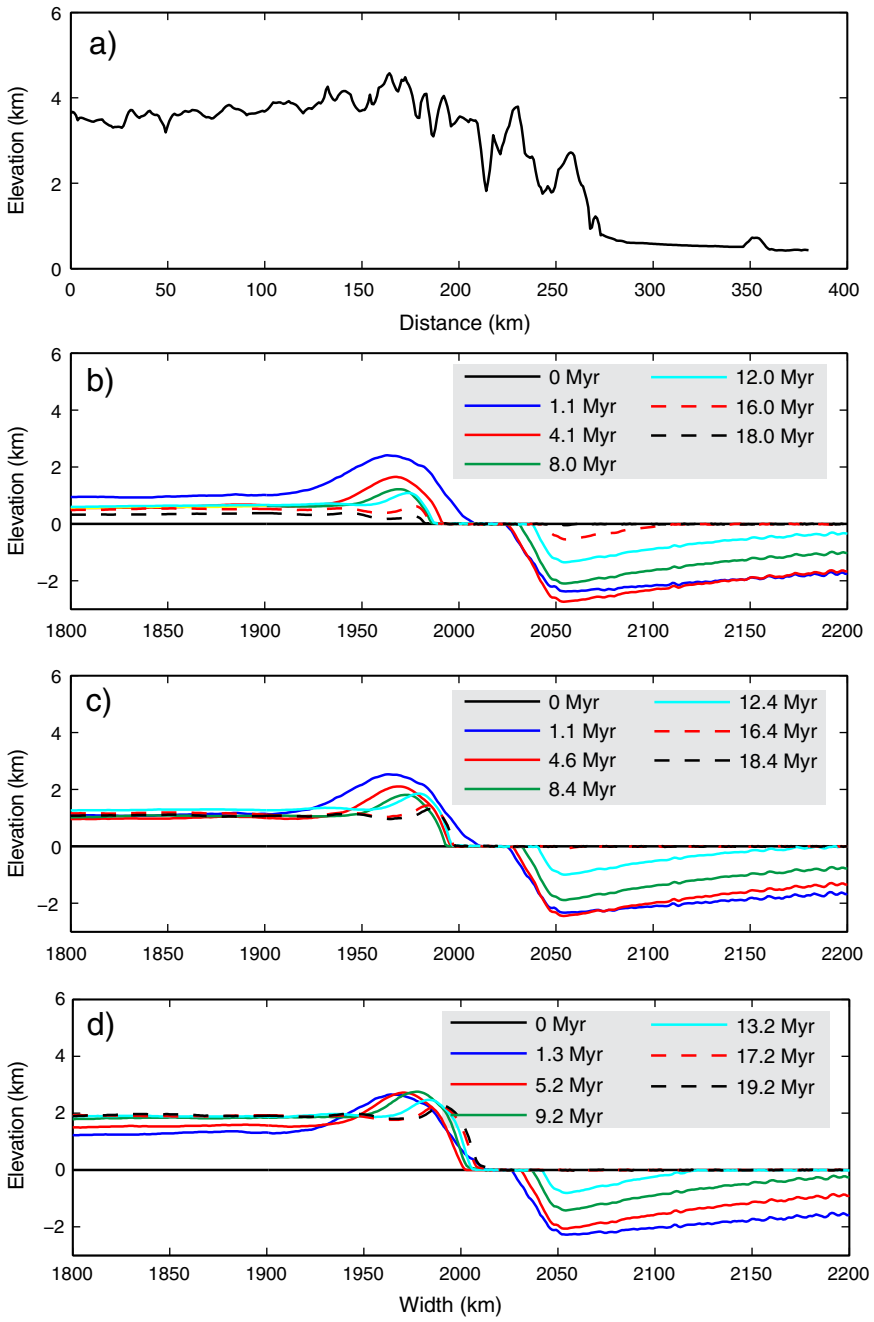

Fig. 8. The comparison between an actual topography and modeled topographies. (a) An actual topography profile across the eastern Tibetan margin. The location of the profile is shown in Fig. 1. The topography profiles at different times with (b) erosion rate = 1.0 mm/a; (c) erosion rate = 0.8 mm/a; (d) erosion rate = 0.6 mm/a. The sediment rates in these models are the same (0.6 mm/a).

other parameters are identical with the reference model (see Table 1 and Fig. 11a). With time few changes are visible in the composition field (see Fig. 11a–d). Even though no pushing force is exerted, several hundred meters of topography uplift are still produced on the left side due to isostasic adjustment resulted from differences in crustal and lithospheric thickness between the two adjacent blocks (see Fig. 12). At the initial stage, the topography increases rapidly, but it approaches a steady state and stops increasing just in 0.78 millions year (see Fig. 12b). If no push is applied on the left side, the maximum height obtained in the plateau is less than 2 km.

This suggested that weak crustal flow model proposed by Royden et al. (1997) is not a necessary condition for the buildup of topography in this region. Beside the convergence rate, the difference in thermal state and lithospheric structure between two interacting blocks plays an important role on mountain building. The high topography gradient of eastern Tibet-type margins may be an inherent feature when a thin and rheologically weak lithosphere with a thick crust interacts directly with a thick and rheologically strong lithosphere with a thin crust.

4. Discussion and conclusion

4.1. Discussion

The eastern Tibetan margin adjacent to the Sichuan basin is characterized by a steep topographic gradient and geophysical differences in thermal state and crustal thickness. The modern high topography of the Longmen Shan and the eastern Tibetan Plateau was probably not established until the Late Cenozoic (Burchfiel et

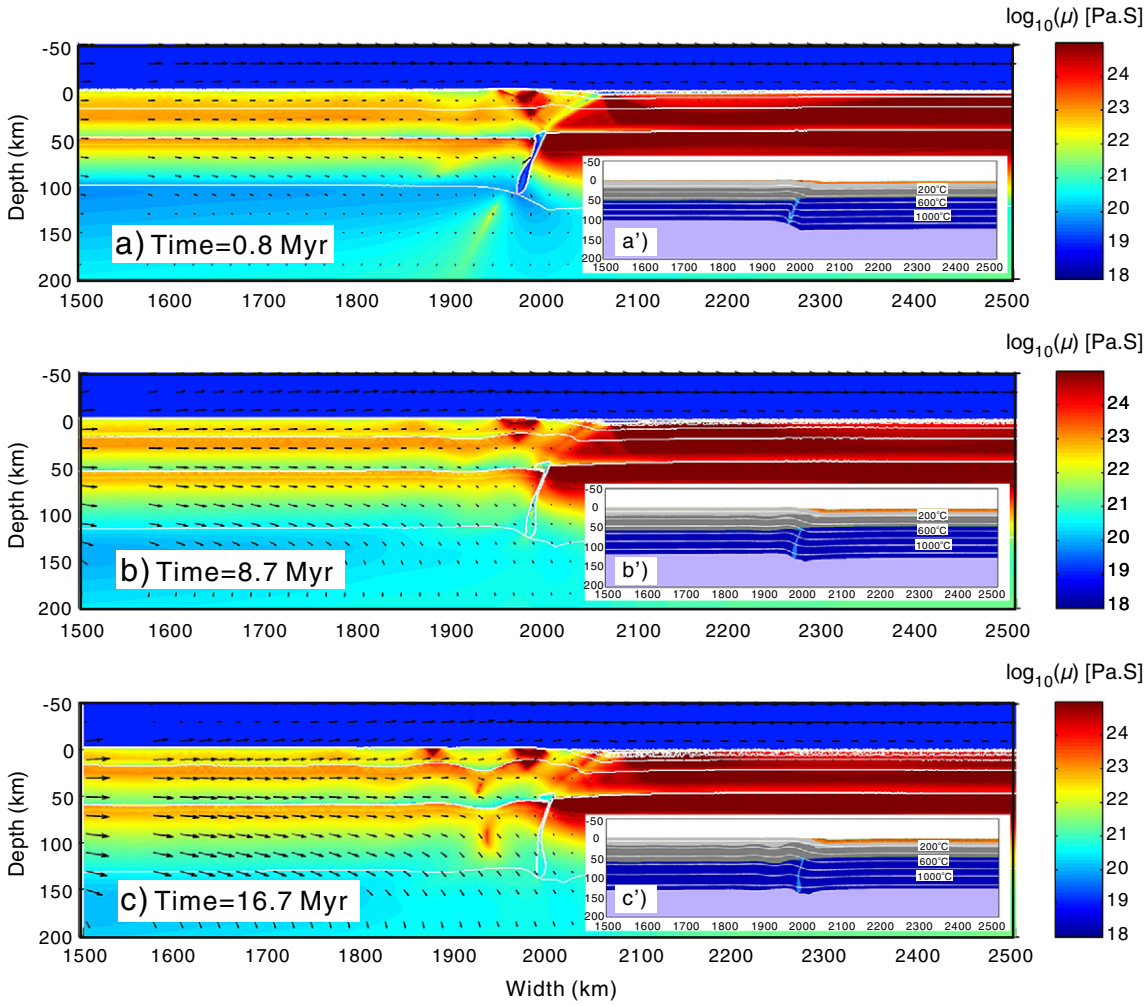

Fig. 9. The composition and viscosity evolution of the model without partially molten crust. Color bars to the right side indicate the magnitude of the viscosity in logarithm. Black arrow indicates the velocity vector and the white lines denote composition contour. The inset images show the composition fields for the same domain with white numbered isothermal lines in °C. The color code of the composition field is the same as in Fig. 2.

al., 2008). Low-temperature isotopic dating indicates that relief along the Longmen Shan developed between 5 and 12 Ma ago (Kirby et al. 2002), while initiation of rapid river incision into the eastern plateau appears to have begun between 8 and 15 Ma (Clark et al. 2005b; Ouimet, 2007). More recently, Wang et al. (2012) used thermochronology to measure the cooling histories of rocks exposed at the eastern Tibet adjacent to the Sichuan Basin. Their results show this margin was subject to slow, steady exhumation during early Cenozoic time, followed by two pulses of rapid exhumation, one beginning 30–25 Ma ago and a second 10–15 Ma ago that continues to present. Even if the exact age and process of the formation of the LMS is still controversial, it is clear that the uplift of the LMS is a fairly recent event. The lower crustal channel flow model (Royden et al., 1997; Clark and Royden, 2000) argues that the eastward flow of weak middle/lower crust material evacuated from central Tibetan Plateau is resisted by the strong and cold Sichuan Basin, leading to an upward inflation of the lower crust and thus the uplift of the LMS range. This model suggests crustal thickening is caused by ductile thickening of the deep crust in a weak layer, thus it does not require large-scale shortening of the upper crust to elevate the LMS. But this model is challenged by a number of recent studies. Seismic anisotropy studies demonstrate that the crust and lithospheric mantle are mechanically coupled in the eastern Tibet region (Lev et al., 2006; Wang et al., 2008; Chen et al., 2012), thus it is unlikely to channelize flow within the lower crust. Based on a precise morphometric analysis of the topography in eastern Tibet, Liu-Zeng et al. (2008) proposed the surface processes, in particular drainage efficiency, coupled with tectonic construction of the relief is an alternative mechanism to explain the bulk topographic characteristics.

Our numerical simulations indicate that the presence of a partially molten crust layer within the middle crust beneath eastern Tibet does not unambiguously decouple the upper crust from the lower lithosphere and a channel flow also does not form. Even in the absence of partially molten crust, a steep topography could be built up through isostatic differences between the converging lithospheres. This suggests that the existence of a partially molten thus mechanically weak middle/lower crust beneath eastern Tibet, which is revealed by seismic and magnetotelluric studies (Bai et al., 2010; Wang et al., 2010), does not necessarily cause channelized flow. Other factors, such as the convergence, material escape, differences in thermal state and crustal thickness, probably play an even more important role in the uplift of the mountain range. The convergence and the differences in temperature and lithospheric structure between adjacent blocks may play an even more important role in building up the topography for the eastern Tibetan-type margin. The pre-existing differences in crustal/lithospheric thickness are likely to result in a contrast of the temperature gradient, thus cause the difference of viscosity. In the context of active orogenic zone like the eastern Tibetan-type margin, a thin lithosphere with a

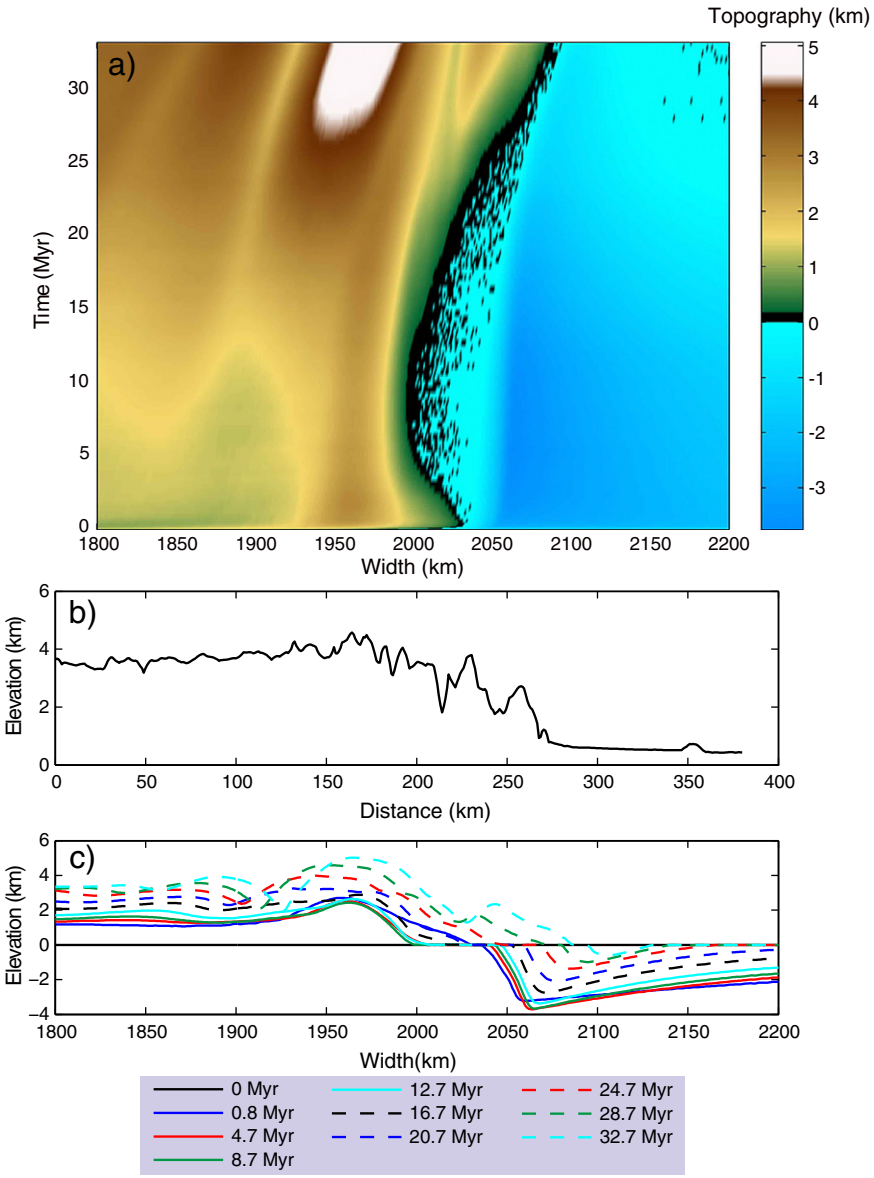

Fig. 10. The topography development of the model without partially molten crust. (a) The topography evolution with time. Colors indicate the magnitude of topography in km. (b) An actual topography profile across the eastern Tibetan margin. The location of the profile is shown in Fig. 1. (c) The topography profiles of the model without partially molten crust at different times.

pre-thickened crust has relatively high geothermal gradient and low viscosity, thus it is weaker and more deformable; while a cratonic lithosphere has relatively low temperature and high viscosity, thus it behaves strong and stiff. The high topography gradient of the eastern Tibet-type margins may be an inherent feature when a thin/hot lithosphere with thick crust converges with a thick lithosphere with thin crust. The occurrence of a shallow fold-and-thrust structure within the upper crust at the conjunction zone of two plates (e.g. Figs. 3 and 9), coupled with pure shear crustal shortening at depth, favors a hybrid tectonic model of weak eastern Tibetan crust overthrusting the Sichuan Basin lithosphere (Tapponnier et al., 2001; Liu-Zeng et al., 2008; Hubbard and Shaw, 2009; Fielding and McKenzie, 2012). Furthermore, Erosion and convergence are two counteracting forces for mountain building (Avouac and Burov, 1996; Willett, 1999; Pysklywec 2006; Liu-Zeng et al., 2008). Erosion plays a destructive role in topography formation, while convergence plays a constructive role. These two interplaying factors together determine the shape and height of a mountain range. In the context of moderate to high erosion rates, the LMS range still gains and maintains a high and steep topography to the present. This could only be explained by exerting a large push force on Tibet side.

The northern Tibetan margin adjacent to the Tarim Basin (see Fig. 1) has many similarities with the eastern Tibetan margin. Both are characterized by steep topographic gradient (Clark and Royden, 2000), little convergence perpendicular to margins (Zhang et al. 2004), existing of major strike-slip faults (Yin and Harrison, 2000), fast P wavespeeds beneath the Tarim Basin (Li et al., 2006), and sharp variation in crustal thickness across the margin (Li, et al., 2001). Thus, these similarities may classify the northern and eastern Tibetan margins as an eastern Tibetan-type margin. According to the above studies, we have reason to speculate that the convergence rate, material escape, and lateral heterogeneities in thermal state and crustal thickness may also play essential

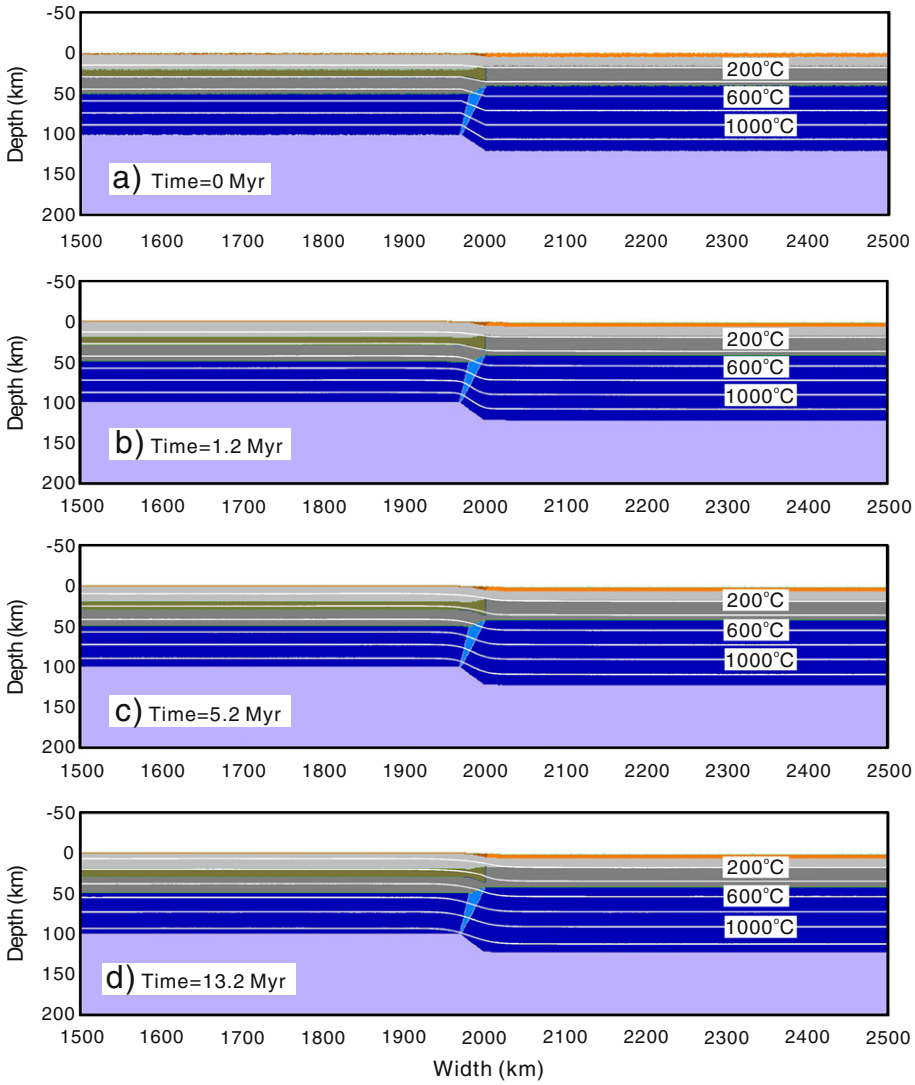

Fig. 11. The composition evolution of the model without push. The color code is the same as in Fig. 2.

roles in the growth of the northern Tibetan margin adjacent to the Tarim Basin, just like the eastern Tibetan margin adjacent to the Sichuan Basin.

It is worth noting that our 2D numerical models just take the boundary-perpendicular convergence into account, and ignore crustal material influx parallel to the margin. Molnar and Tapponnier (1975) argued that during the south–north collision between the Indian and Eurasian plates, the crustal material of eastern Tibet escaped southeast along several strike-slip faults due to the obstacle of the rigid Sichuan Basin. The south-east escape of crustal material of eastern Tibet may partake in the convergence. Clark et al. (2005a) used a rigid cylinder to approximate the rigid Sichuan Basin standing against the crustal flow. Cook and Royden (2008) investigate the effects of lateral strength heterogeneities in the crust on the patterns of uplift in collisional orogens using three dimensional thin sheet model. They treat the Sichuan and Tarim Basins as regions with high viscosity. These studies indicate that lateral variation of viscosity in the crust has a dramatic effect on the morphology and dynamics of plateau growth. As mentioned above, these models based on thin sheet model are too simplified to account for the complexity of the dimensional crustal channel flow. Further study should focus on 3D numerical modeling of this type of margins with petrological-thermomechanical model. The south-east escape of crustal material of eastern Tibet may contribute to the strikingly slow surface convergence rate revealed by GPS measurement.

4.2. Conclusion

We investigated several major factors responsible for mountain building, such as the convergence rate, the erosion/sediment rate, and the presence of a partially molten middle/lower crust. The numerical experiments show that:

1. Topography differences across the eastern Tibetan-type margins are mainly derived from isostatic equilibration forces that account for differences in crustal and lithospheric thickness. The rigid cratonic lithosphere is resistant to deformation (thickening), thus crustal thickening and topography growth is focused on the Tibet side.
2. Significant convergence (or some other crustal thickening processes) is necessary to build and maintain high topography in the presence of moderate to high erosion rates.

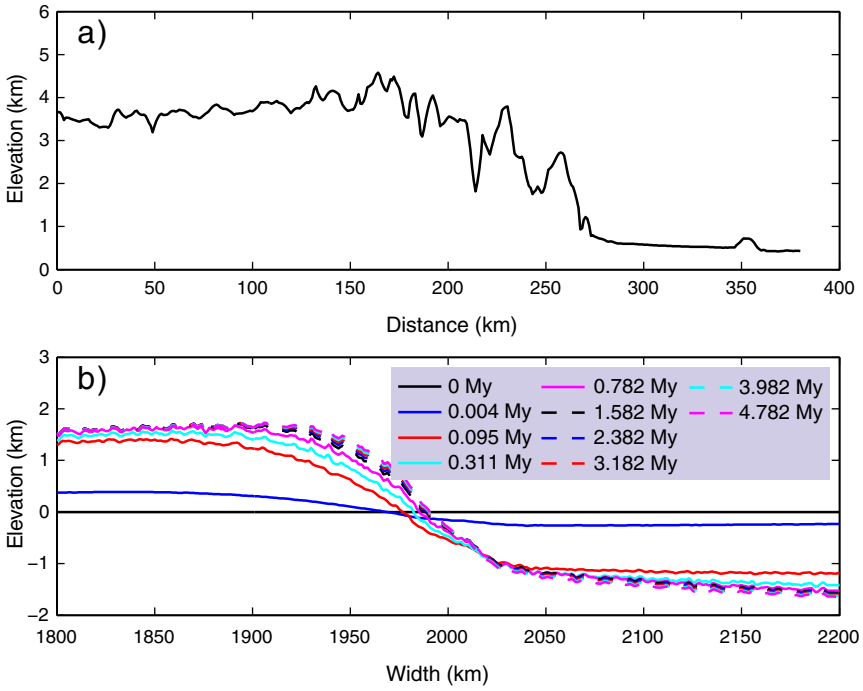

Fig. 12. The comparison between an actual topography and modeled topographies. (a) An actual topography profile across the eastern Tibetan margin. The location of the profile is shown in Fig. 1. (b) The topography profiles of the model without push at different times.

3. The role of a partially molten middle/lower crust significantly modifies the shape of topography, but it is not necessary for steep topography growth.

Acknowledgment

This research was supported by the National Natural Science Foundation of China (no. 41004039 and 41021063) and the Ministry of Science and Technology and the Ministry of the Land and Resources (Sinoprobe-02-02 or no. 201111041). We thank Harro Schmeling for his constructive suggestions. We thank Chen Qu, Huang Fang, Wang Jingtao, Wei Xing and Katharina Vogt for their assistance during Lin's stay in ETH. We are very grateful to two anonymous reviewers and the associate editor, Dr. Alan R.A. Aitken, for their constructive comments, which significantly improved the clarity and presentation of the results. We are grateful to Dr. Yun Chen for his help on drawing Fig. 1. All the simulations were run on the ETH Brutus cluster.

Appendix A

Equations

The momentum, continuity and heat conservation equations for a 2D creeping flow including thermal and chemical buoyant forces are solved with the I2VIS code (Gerya and Yuen, 2003a). The 2D Stokes equation has the form:

$$\frac{\partial \sigma_{xx}}{\partial x}+\frac{\partial \sigma_{xz}}{\partial z}=\frac{\partial P}{\partial x} \tag{1}$$

$$\frac{\partial \sigma_{zz}}{\partial z}+\frac{\partial \sigma_{zx}}{\partial x}=\frac{\partial P}{\partial z}-g\rho(T,P,C,M) \tag{2}$$

where σ_{xx}, σ_{xz} and σ_{zz} are the deviatoric stress tensor components. The density ρ depends on temperature (T), pressure (P), composition (C) and mineralogy (M). g is the acceleration due to gravity.

Conservation of mass is approximated by the incompressible continuity equation:

$$\frac{\partial v_x}{\partial x}+\frac{\partial v_z}{\partial z}=0 \tag{3}$$

where v_x and v_z are the horizontal and vertical component of velocity vector respectively.

The heat conversation equation takes the form:

$$\rho C_p\left(\frac{DT}{Dt}\right)=-\frac{\partial q_x}{\partial x}-\frac{\partial q_z}{\partial z}+H_r+H_a+H_S+H_L \tag{4}$$

$$q_x=-k(T,P,C)\frac{\partial T}{\partial x} \tag{5}$$

$$q_z=-k(T,P,C)\frac{\partial T}{\partial z} \tag{6}$$

$$H_a=T\alpha\frac{DP}{Dt} \tag{7}$$

$$H_S=\sigma_{xx}\varepsilon_{xx}+\sigma_{zz}\varepsilon_{zz}+2\sigma_{xz}\varepsilon_{xz} \tag{8}$$

where D/Dt is the substantive time derivative; x an z denote the horizontal and vertical directions respectively; ε_{xx}, ε_{xz} and ε_{zz} are the components of strain rate tensor; q_x and q_z are heat flux components; $k(T,P,C)$ is the thermal conductivity as a function of temperature, pressure and composition; C_p is the isobaric heat capacity; H is the rock enthalpy at the current time step; H_r, H_a, H_s, H_L are radioactive, adiabatic, shear and latent heat production, respectively (see Table 2 for details of these parameters).

Topography

The spontaneous deformation of the upper surface, i.e. topography, is calculated dynamically as a free surface by using a low viscosity (10^{19} Pa s) sticky “air” layer (50 km thick in our experiments).

The interface between this weak layer and the underlying crust is treated as an erosion/sediment surface which evolves according to the transportation equation (Gerya and Yuen, 2003b):

$$\frac{\partial z_{es}}{\partial t} = v_z - v_x \frac{\partial z_{es}}{\partial x} - v_s + v_e \tag{9}$$

where z_{es} is the vertical position of the surface as a function of the horizontal distance; v_z and v_x are the vertical and horizontal components of the material velocity vector at the surface; v_s and v_e are the sediment and erosion rates, respectively.

Rheological model

The rheologies used in the experiments are visco-plastic. Viscous creep is computed in terms of deformation invariants and depends on strain rate, temperature, and pressure (Ranalli, 1995). The viscous component of the deformation is calculated as a combination of diffusion (η_{dif}) and dislocation creep (η_{dis}):

$$\frac{1}{\eta_{\text{creep}}} = \frac{1}{\eta_{dif}} + \frac{1}{\eta_{dis}} \tag{10}$$

The calculation of the viscosity associated with dislocation creep regime is formulated as follows:

$$\eta_{\text{creep}} = (\dot{\varepsilon}_{II})^{(1-n)/2n} (A)^{-1/n} \times \exp\left(\frac{E_a + PV_a}{nRT}\right) \tag{11}$$

where $\dot{\varepsilon}_{II}$ is the second invariant of strain rate; A, E_a, V_a, n are material constant, activation energy, activation volume and stress exponent, respectively. These material properties are determined from laboratory flow experiments and are given in Table 2. A smooth transition between diffusion creep and dislocation creep is assumed to occur at approximately 30 kPa (Turcotte and Schubert, 1982). By equating strain rate invariants for dislocation creep and diffusion creep at the stress transition, an expression for diffusion creep viscosity is derived as a function of the dislocation creep flow law.

Plasticity is implemented using the Druker–Prager yield criterion (Ranalli, 1995). The calculated creep viscosity is limited in the following manner:

$$\eta_{\text{creep}} \leq \frac{C + P\sin(\phi)}{(4\dot{\varepsilon}_{II})^{1/2}} \tag{12}$$

where C is the cohesion and ϕ is the internal angle of friction.

Viscous rheology for rocks containing small melt fractions ($M<0.1$) is determined by flow laws (Eqs. (11)–(12)). The effective viscosity of molten rocks ($M>0.1$) was calculated using the formula (Pinkerton and Stevenson, 1992; Bittner and Schmeling, 1995):

$$\eta = \eta_0 \exp\left[2.5 + (1-M)\left(\frac{1-M}{M}\right)^{0.48}\right] \tag{13}$$

where η_0 is an empirical parameter depending on rock composition, being $\eta_0 = 10^{13}$ Pa s for molten mafic rocks and $\eta_0 = 5\times10^{14}$ Pa s for molten felsic rocks.

Partial melting

The numerical code accounts for partial melting of the various lithologies by using experimentally obtained P-T dependent wet solidus and dry liquidus curves (Table 2). Volumetric melt fraction M is assumed to increase linearly with temperature according to the following relations (Burg and Gerya, 2005):

$$M = \begin{cases} 0, & T \leq T_{solidus} \\ \dfrac{T - T_{solidus}}{T_{liquidus} - T_{solidus}}, & T_{solidus} < T < T_{liquidus} \\ 1, & T \geq T_{liquidus} \end{cases} \tag{14}$$

where $T_{solidus}$ and $T_{liquidus}$ are the wet solidus and dry liquidus temperature of a given lithology, respectively.

Consequently, the effective density, ρ_{eff}, of partially molten rocks varies with the amount of melt fraction and P-T conditions according to the relations:

$$\rho_{eff} = \rho_{solid} - M(\rho_{solid} - \rho_{molten}) \tag{15}$$

$$\rho_{P,T} = \rho_0[1 - \alpha(T - T_0)][1 + \beta(P - P_0)] \tag{16}$$

where ρ_{solid} and ρ_{molten} are the densities of the solid and molten rock respectively; ρ_0 is the density at $P_0 = 0.1$ MPa and $T_0 = 298$ K; α and β are the thermal expansion and compressibility coefficients, respectively.

The effects of latent heat are accounted for by an increased effective heat capacity (C_{pe}) and thermal expansion (α_e) of the partially molten rocks ($0<M<1$), calculated as follows:

$$C_{pe} = C_p + Q_L\left[(\partial M/\partial T)_P\right] \tag{17}$$

$$\alpha_e = \alpha + \rho Q_L\left[(\partial M/\partial P)_T\right]/T \tag{18}$$

where C_p and α are the heat capacity and the thermal expansion of the solid rock respectively, and Q_L is the latent heat of melting rock.

References

Aitchison, J.C., Ali, J.R., Davis, A., 2007. When and where did India and Asia collide? Journal of Geophysical Research 112, B05423. http://dx.doi.org/10.1029/2006JB004706.

Aitchison, J.C., Xia, X., Baxter, A.T., Ali, J.R., 2011. Detrital zircon U–Pb ages along the Yarlung–Tsangpo suture zone, Tibet: implications for oblique convergence and collision between India and Asia. Gondwana Research. http://dx.doi.org/10.1016/j.gr.2011.04.002.

Arne, D., Worley, B., Wilson, C., Chen, S.F., Foster, D., Luo, Z.L., Liu, S.G., Dirks, P., 1997. Differential exhumation in response to episodic thrusting along the eastern margin of the Tibetan Plateau. Tectonophysics 280, 239–256.

Avouac, J.P., Burov, E.B., 1996. Erosion as a driving mechanism of intracontinental mountain growth. Journal of Geophysical Research 101, 17747–17769.

Bai, D., Unsworth, M.J., Meju, M.A., Ma, X., Teng, J., Kong, X., Sun, Y., Sun, J., Wang, L., Jiang, C., Zhao, C., Xiao, P., Liu, M., 2010. Crustal deformation of the eastern Tibetan plateau revealed by magnetotelluric imaging. Nature Geoscience 3, 358–362.

Bai, Z., Tian, X., Tian, Y., 2011. Upper mantle P-wave tomography across the Longmenshan fault belt from passive-source seismic observations along Aba-Longquanshan profile. Journal of Asian Earth Sicences 40, 873–882.

Bird, P., 1991. Lateral extrusion of lower crust from under high topography, in the isostatic limit. Journal of Geophysical Research 96, 10275–10286.

Bittner, D., Schmeling, H., 1995. Numerical modelling of melting processes and induced diapirism in the lower crust. Geophysical Journal International 123, 59–70.

Braitenberg, C., Wang, Y., Fang, J., Hsu, H., 2003. Spatial variations of flexure parameters over the Tibet–Qinghai plateau. Earth and Planet Science Letters 205, 211–224.

Burchfiel, B.C., Chen, Z., Liu, Y., Royden, L., 1995. Tectonics of the Longmen Shan and adjacent regions, Central China. International Geology Review 37, 661–735.

Burchfiel, B.C., Royden, L.H., van der Hilst, R.D., Hager, B.H., Chen, Z., King, R.W., Li, C., Lu, J., Yao, H., Kirby, E., 2008. A geological and geophysical context for the Wenchuan earthquake of 12 May 2008, Sichuan, People's Republic of China. GSA Today 18. http://dx.doi.org/10.1130/GSATG18A.1.

Burg, J.P., Gerya, T.V., 2005. The role of viscous heating in Barrovian metamorphism of collisional orogens: thermomechanical models and application to the Lepontine Dome in the Central Alps. Journal of Metamorphic Geology 23, 75–95.

Chen, Z., Burchfiel, B.C., Liu, Y., King, R.W., Royden, L.H., Tang, W., Wang, E., Zhao, J., Zhang, X., 2000. Global positioning system measurements from eastern Tibet and their implications for India/Eurasia intercontinental deformation. Journal of Geophysical Research 105, 16215–16227.

Chen, Y., Zhang, Z., Sun, C., Badal, J., 2012. Crustal anisotropy from Moho converted Ps wave splitting analysis and geodynamic implications beneath the eastern margin of Tibet and surrounding regions. Gondwana Research. http://dx.doi.org/10.1016/j.gr.2012.04.003.

Chung, S.-L., Chu, M.-F., Zhang, Y., Xie, Y., Lo, C.-H., Lee, T.-Y., Lan, C.-Y., Li, X., Zhang, Q., Wang, Y., 2005. Tibetan tectonic evolution inferred from spatial and temporal variations in post-collisional magmatism. Earth-Science Reviews 68, 173–196.

Clark, M.K., Royden, L.H., 2000. Topographic ooze: building the eastern margin of Tibet by lower crustal flow. Geology 28, 703–706.
Clark, M.K., Bush, J.M., Royden, L.H., 2005a. Dynamic topography produced by lower crustal flow against rheological strength heterogeneities bordering the Tibetan Plateau. Geophysical Journal International 162, 575–590.
Clark, M.K., House, M.A., Royden, L.H., Burchfiel, B.C., Whipple, K.X., Zhang, X., Tang, W., 2005b. Late Cenozoic uplift of southeastern Tibet. Geology 33, 525–528.
Cook, K.L., Royden, L.H., 2008. The role of crustal strength variations in shaping orogenic plateaus, with application to Tibet. Journal of Geophysical Research 113, B08407. http://dx.doi.org/10.1029/2007JB005457.
Copley, A., McKenzie, D., 2007. Models of crustal flow in the India–Asia collision zone. Geophysical Journal International 169, 683–698.
Dai, J., Zhao, X., Wang, C., Zhu, L., Li, Y., Finn, D., 2012. The vast proto-Tibetan Plateau: new constraints from Paleogene Hoh Xil Basin. Gondwana Research 22, 434–446.
Dewey, J.F., Shackleton, R.M., Chang, C., Sun, Y., 1988. The tectonic evolution of the Tibetan Plateau. Philosophical Transactions of the Royal Society of London A 327, 379–413.
Duretz, T., Gerya, T.V.,May, D.A., in press. Numerical modelling of spontaneous slab breakoff and subsequent topographic response. Tectonophysics. http://dx.doi.org/10.1016/j.tecto.2010.05.024.
England, P., Houseman, G., 1986. Finite strain calculations of continental deformation 2. Comparison with the India–Asia collision zone. Journal of Geophysical Research 91, 3664–3676.
England, P., McKenzie, D., 1982. A thin viscous sheet model for continental deformation. Geophysical Journal of the Royal Astronomical Society 70, 295–321.
Fielding, E.J., McKenzie, D., 2012. Lithospheric flexure in the Sichuan Basin and Longmen Shan at the eastern edge of Tibet. Geophysical Research Letters 39, L09311. http://dx.doi.org/10.1029/2012GL051680.
Fielding, E., Isacks, B., Barazangi, M., Duncan, C., 1994. How flat is Tibet? Geology 22, 163–167.
Gan, W., Zhang, P., Shen, Z., Niu, Z., Wang, M., Wan, Y., Zhou, D., Cheng, J., 2007. Present-day crustal motion within the Tibetan Plateau inferred from GPS measurements. Journal of Geophysical Research 112, B08416. http://dx.doi.org/10.1029/2005JB004120.
Gerya, T.V., 2010. Introduction to Numerical Geodynamic Modelling. Cambridge University Press, London UK, p. 338.
Gerya, T.V., Stockhert, B., 2006. Two-dimensional numerical modeling of tectonic and metamorphic histories at active continental margins. International Journal of Earth Science 95, 250–274.
Gerya, T.V., Yuen, D.A., 2003a. Characteristics-based marker-in-cell method with conservative finite-differences schemes for modeling geological flows with strongly variable transport properties. Physics of Earth and Planetary Interiors 140, 295–320.
Gerya, T.V., Yuen, D.A., 2003b. Rayleigh–Taylor instabilities from hydration and melting propel 'cold plumes' at subduction zones. Earth and Planetary Science Letters 212, 47–62.
Gerya, T.V., Yuen, D.A., Maresch, W., 2004a. Thermomechanical modelling of slab detachment. Earth and Planetary Science Letters 226, 101–116.
Gerya, T.V., Yuen, D.A., Sevre, E.D., 2004b. Dynamical causes for incipient magma chambers above slabs. Geology 32, 89–92.
Gerya, T.V., Yuen, D.A., 2007. Robust characteristics method for modelling multiphase visco-elasto-plastic thermo-mechanical problems. Physics of the Earth and Planetary Interiors 163, 83–105.
Gerya, T.V., Perchuk, L.L., Burg, J.P., 2008. Transient hot channels: perpetrating and regurgitating ultrahigh-pressure, high-temperature crust-mantle associations in collision belts. Lithos 103, 236–256.
Godard, V., Cattin, R., Lave, J., 2009a. Erosional control on the dynamics of low-convergence rate continental plateau margins. Geophysical Journal International 179, 763–777.
Godard, V., Pik, R., Lave, J., Cattin, R., Tibari, B., de Sigoyer, J., Pubellier, M., 2009b. Late Cenozoic evolution of the central Longmen Shan, eastern Tibet: Insight from (U-Th)/He thermochronometry. Tectonics 28, TC5009. http://dx.doi.org/10.1029/2008TC002407.
Gratton, J., 1989. Crustal shortening, root spreading, isostasy, and the growth of orogenic belts: a dimensional analysis. Journal of Geophysical Research 94, 15627–15634.
Holbig, E.S., Grove, T.L., 2008. Mantle melting beneath the Tibetan Plateau: experimental constraints on ultrapotassic magmatism. Journal of Geophysical Research 113, B04210. http://dx.doi.org/10.1029/2007JB005149.
Houseman, G., England, P., 1993. Crustal thickening versus lateral expulsion in the Indian–Asian continental collision. Journal of Geophysical Research 98, 12233–12249.
Hubbard, J., Shaw, J.H., 2009. Uplift of the Longmen Shan and Tibetan plateau, and the 2008 Wenchuan (M = 7.9) earthquake. Nature 458, 194–197.
Jiang, X., Jin, Y., 2005. Mapping the deep lithospheric structure beneath the eastern margin of the Tibetan Plateau from gravity anomalies. Journal of Geophysical Research 110, B07407. http://dx.doi.org/10.1029/2004JB003394.
Johnson, M.R.W., 2002. Shortening budgets and the role of continental subduction during the India–Asia collision. Earth-Science Reviews 59, 101–123.
Kirby, E., Reiners, P.W., Krol, M.A., Whipple, K.X., Hodges, K.V., Farley, K.A., Tang, W., Chen, Z., 2002. Late Cenozoic evolution of the eastern margin of the Tibetan Plateau: Inferences from $^{40}Ar/^{39}Ar$ and (U–Th)/He thermochronology. Tectonics 21. http://dx.doi.org/10.1029/2000TC001246.
Lai, Q.Z., Ding, L., Wang, H.W., Yue, Y.H., Cai, F.L., 2007. Constraining the stepwise migration of the eastern Tibetan Plateau margin by apatite fission track thermochronology. Science in China Series D: Earth Sciences 50, 172–183.
Lei, J., Zhao, D., 2009. Structural heterogeneity of the Longmenshan fault zone and the mechanism of the 2008 Wenchuan earthquake (Ms 8.0). Geochemistry, Geophysics, Geosystems 10, Q10010. http://dx.doi.org/10.1029/2009GC002590.
Lev, E., Long, M.D., van der Hilst, R.D., 2006. Seismic anisotropy from shear-wave splitting in Eastern Tibet reveals changes in lithospheric deformation. Earth and Planet Science Letters 251, 293–304.
Li, Q.S., Lu, D.Y., Gao, R., Zhang, Z.Y., Liu, W., Li, Y.K., Li, J.W., Fan, J.Y., Xiong, X.M., 2001. An integrated study of deep seismic sounding profile along Xinjiang Global Geoscience Transect (Quanshuigou-Dushanzi). Acta Geoscientia Sinica 22, 534–540 (in Chinese with English Abstract).
Li, C., van der Hilst, R.D., Toksoz, M.N., 2006. Constraining spatial variations in P-wave velocity in the upper mantle beneath SE Asia. Physics of Earth and Planetary Interiors 154, 180–195.
Li, C., van der Hilst, R.D., Engdahl, E.R., Burdick, S., 2008. A new global model for P-wave speed variations in Earth's mantle. Geochemistry, Geophysics, Geosystems. http://dx.doi.org/10.1029/2007GC001806.
Li, Y., Jia, D., Shaw, J.H., Hubbard, J., Lin, A., Wang, M., Luo, L., Li, H., Wu, L., 2010. Structural interpretation of the coseismic faults of the Wenchuan earthquake: three-dimensional modelling of the Longmen Shan fold-and-thrust belt. Journal of Geophysical Research 115, B04317. http://dx.doi.org/10.1029/2009JB006824.
Li, Z.-W., Liu, S., Chen, H., Deng, B., Hou, M., Wu, W., Gao, J., 2012a. Spatial variation in Meso-Cenozoic exhumation history of the Longmen Shan thrust belt (eastern Tibetan Plateau) and the adjacent western Sichuan basin: constraints from fission tract thermochronology. Journal of Asian Earth Science 47, 185–203.
Li, Z., Ni, S., Hao, T., Xu, Y., Roecker, S., 2012b. Uppermost mantle structure of the eastern margin of the Tibetan Plateau from interstation Pn traveltime difference tomography. Earth and Planetary Science Letters 335–336, 195–205.
Liu, M., Yang, Y., 2003. Extensional collapse of the Tibetan Plateau: Results of three-dimensional finite element modeling. Journal of Geophysical Research 108 (B8), 2361. http://dx.doi.org/10.1029/2002JB002248.
Liu-Zeng, J., Tapponnier, P., Gaudemer, Y., Ding, L., 2008. Quantifying landscape differences across the Tibetan plateau: implications for topographic relief evolution. Journal of Geophysical Research 113, F04018. http://dx.doi.org/10.1029/2007JF000897.
Liu-Zeng, J., Wen, L., Oskin, M., Zeng, L., 2011. Focused modern denudation of the Longmen Shan margin, eastern Tibetan Plateau. Geochemistry, Geophysics, Geosystems 12, Q11007. http://dx.doi.org/10.1029/2011GC003652.
Maidment, D.W., Hand, M., Williams, I.S., 2013. High grade metamorphism of sedimentary rocks during Palaeozoic rift basin formation in central Australia. Gondwana Research 24, 865–885.
Mechie, J., Kind, R., Saul, J., 2011. The seismological structure of the Tibetan Plateau crust and mantle down to 700 km depth. In: Gloaguen, R., Ratschbacher, L. (Eds.), Growth and Collapse of the Tibetan Plateau: Geological Society of London Special Publications, 353, pp. 109–125.
Meng, Q.R., Hu, J.M., Wang, E., Qu, H.J., 2006. Late Cenozoic denudation by large-magnitude landslides in eastern edge of Tibetan Plateau. Earth and Planetary Science Letters 243, 252–267.
Molnar, P., 1988. A review of geophysical constraints on the deep structure of the Tibetan Plateau, the Himalaya and the Karakoram, and their tectonic implications. Philosophical Transactions of Royal Society of London A 326, 33–88.
Molnar, P., Stock, J.M., 2009. Slowing of India's convergence with Eurasia since 20 Ma and its implications for Tibetan mantle dynamics. Tectonics 28, TC3001. http://dx.doi.org/10.1029/2008TC002271.
Molnar, P., Tapponnier, P., 1975. Cenozoic tectonics of Asia: effects of a continental collision. Science 189, 419–426.
Molnar, P., England, P., Martinod, J., 1993. Mantle dynamics, uplift of the Tibetan Plateau and the Indian monsoon. Reviews of Geophysics 31, 357–396.
Ouimet, W., 2007. Dissecting the eastern margin of the Tibetan Plateau: A study of landslides, erosion and river incision in a transient landscape. Ph.D. thesis, Cambridge, Massachusetts Institute of Technology, 197 pp.
Pinkerton, H., Stevenson, R.J., 1992. Methods of determining the rheological properties of magmas at subliquidus temperatures. Journal of Volcanology and Geothermal Research 53, 47–66.
Pysklywec, R.N., 2006. Surface erosion control on the evolution of the deep lithosphere. Geology 34, 225–228.
Ranalli, G., 1995. Rheology of the Earth, 2nd ed. Chapman & Hall, London, p. 413.
Robert, A., Zhu, J., Vergne, J., Cattin, R., Chan, L.S., Wittlinger, G., Herquel, G., de Sigoyer, J., Pubellier, M., Zhu, L.D., 2010. Crustal structures in the area of the 2008 Sichuan earthquake from seismologic and gravimetric data. Tectonophysics 491, 205.
Royden, L.H., Burchfiel, B.C., King, R.W., Wang, E., Chen, Z., Shen, F., Liu, Y., 1997. Surface deformation and lower crustal flow in eastern Tibet. Science 276, 788–790.
Schmeling, H., Babeyko, A.Y., Enns, A., Faccenna, C., Funiciello, F., Gerya, T., Golabek, G.J., Grigull, J., Kaus, B.J.P., Morra, G., Schmalholz, S.M., van Hunen, J., 2008. A benchmark comparison of spontaneous subduction models: towards a free surface. Physics of Earth and Planetary Interiors 171, 198–223.
Searle, M.P., Elliott, J.R., Phillips, R.J., Chung, S.-L., 2011. Crustal-lithospheric structure and continental extrusion of Tibet. Journal of the Geological Society of London 168, 633–672.
Tapponnier, P., Xu, Z.Q., Roger, F., Meyer, B., Arnaud, N., Wittlinger, G., Yang, J., 2001. Oblique stepwise rise and growth of the Tibet Plateau. Science 294, 1671–1677.
Turcotte, D.L., Schubert, G., 1982. Geodynamics: Applications of Continuum Physics to Geological Problems. Wiley, New York, p. 450.
van Hinsbergen, D.J.J., Lippert, P.C., Dupont-Nivet, G., McQuarrie, N., Doubrovine, P.V., Spakman, W., Torsvik, T.H., 2012. Greater India Basin hypothesis and a two-stage Cenozoic collision between India and Asia. PNAS 109, 7659–7664. http://dx.doi.org/10.1073/pnas.1117262109.
Wallis, S., Tsujimori, T., Aoya, M., Kawakami, T., Terada, K., Suzuki, K., Hyodo, H., 2003. Cenozoic and Mesozoic metamorphism in the Longmenshan orogen: implications for geodynamic models of eastern Tibet. Geology 31, 745–748.

Wang, E.C., Meng, Q.R., 2009. Mesozoic and Cenozoic tectonic evolution of the Longmenshan fault belt. Science in China Series D: Earth Sciences 52, 579–592.
Wang, C.Y., Han, W.B., Wu, J.P., Lou, H., Chan, W.W., 2007. Crustal structure beneath the eastern margin of the Tibetan Plateau and its tectonic implications. Journal of Geophysical Research 112, B07307. http://dx.doi.org/10.1029/2005JB003873.
Wang, C.Y., Flesch, L.M., Silver, P.G., Chang, L.J., Chan, W.W., 2008. Evidence for mechanically coupled lithosphere in central Asia and resulting implications. Geology 36 (5), 363–366. http://dx.doi.org/10.1130/G24450A.
Wang, C.Y., Lou, H., Silver, P.G., Zhu, L., Chang, L., 2010. Crustal structure variation along 30 N in the eastern Tibetan Plateau and its tectonic implications. Earth and Planetary Science Letters 289, 367–376.
Wang, E., Kirby, E., Furlong, K.P., van Soest, M., Xu, G., Shi, X., Kamp, P.J.J., Hodges, K.V., 2012. Two-phase growth of high topography in eastern Tibet during the Cenozoic. Nature Geoscience. http://dx.doi.org/10.1038/NGEO1538.
Willett, S.D., 1999. Orogeny and orography: the effects of erosion on the structure of mountain belts. Journal of Geophysical Research 104, 28957–28981.
Xia, L., Li, X., Ma, Z., Xu, X., Xia, Z., 2011. Cenozoic volcanism and tectonic evolution of the Tibetan plateau. Gondwana Research 19, 850–866.
Xu, M., Zhu, C.Q., Rao, S., Hu, S.B., 2011. Difference of thermal structure between eastern edge of Tibet Plateau and western Sichuan Basin. Chinese Journal of Geology 46, 203–212 (in Chinese with English abstract).
Xu, Z., Ji, S., Cai, Z., Zeng, L., Geng, Q., Cao, H., 2012. Kinematics and dynamics of the Namche Barwa Syntaxis, eastern Himalaya: constraints from deformation, fabrics and geochronology. Gondwana Research 21, 19–36.
Yang, Y., Liu, M., 2009. Crustal thickening and lateral extrusion during the Indo-Asian collision: a 3D viscous flow model. Tectonophysics 465, 128–135.
Yin, A., 2010. A special issue on the great 12 May 2008 Wenchuan earthquake (Mw7.9): observations and unanswered questions. Tectonophysics 491, 1–9.
Yin, A., Harrison, T.M., 2000. Geological evolution of the Himalayan Tibetan orogen. Annual Review of Earth and Planetary Science 28, 211–280.
Yuan, Y.S., Ma, Y.S., Hu, S.B., Guo, T.L., Fu, X.Y., 2006. Present-day geothermal characteristics in South China. Chinese Journal of Geophysics 49, 1118–1126 (in Chinese with English abstract).
Zhang, Z., Klemperer, S.L., 2010. Crustal structure of the Tethyan Himalaya, southern Tibet: new constraints from old wide-angle seismic data. Geophysical Journal International 181, 1247–1260.
Zhang, P., Shen, Z., Wang, M., Gan, W., Burgmann, R., Molnar, P., 2004. Continuous deformation of the Tibetan Plateau from global positioning system data. Geology 32, 809–812.
Zhang, Z., Wang, Y., Chen, Y., Houseman, G.A., Tian, X., Wang, E., Teng, J., 2009. Crustal structure across Longmenshan fault belt from passive source seismic profiling. Geophysical Research Letters 36, L17310. http://dx.doi.org/10.1029/2009GL039580.
Zhang, Z., Yuan, X., Chen, Y., Tian, X., Kind, R., Li, X., Teng, J., 2010. Seismic signature of the collision between the East Tibetan escape flow and the Sichuan basin. Earth and Planetary Sciences Letters 292, 254–264.
Zhang, Z., Deng, Y., Teng, J., Wang, C., Gao, R., Chen, Y., Fan, W., 2011a. An overview of the crustal structure of the Tibetan plateau after 35 years of deep seismic soundings. Journal of Asian Earth Sciences 40, 977–989.
Zhang, Z.J., Klemperer, S.L., Bai, Z.M., Chen, Y., Teng, J.W., 2011b. Crustal structure of the Paleozoic Kunlun orogeny from an active-source seismic profile between Moba and Guide in East Tibet, China. Gondwana Research 19, 994–1007.
Zhang, Z.J., Yang, L.Q., Teng, J.W., Badal, J., 2011c. An overview of the earth crust under China. Earth-Science Reviews 104, 143–166.
Zhang, Z., Deng, Y., Chen, L., Wu, J., Teng, J., Panza, G., 2012. Seismic structure and rheology of the crust beneath mainland China. Gondwana Research. http://dx.doi.org/10.1016/j.gr.2012.07.010.